

# A Cenozoic record of seawater uranium in fossil corals

Anne M. Gothmann <sup>a,b,\*</sup>, John A. Higgins <sup>a</sup>, Jess F. Adkins <sup>c</sup>, Wally Broecker <sup>d</sup>, Kenneth A. Farley <sup>c</sup>, Ryan McKeon <sup>c</sup>, Jarosław Stolarski <sup>e</sup>, Noah Planavsky <sup>f</sup>, Xiangli Wang <sup>f,g,h</sup>, Michael L. Bender <sup>a</sup>

<sup>a</sup> Princeton University, Department of Geosciences, Guyot Hall, Princeton, NJ 08542, USA

<sup>b</sup> St. Olaf College, Departments of Environmental Studies and Physics, Northfield, MN 55057, USA

<sup>c</sup> California Institute of Technology, Division of Geological and Planetary Sciences, MC 100-23, 1200 E. California Blvd, Pasadena, CA 91125, USA

<sup>d</sup> Lamont-Doherty Earth Observatory of Columbia University, Palisades, NY 10964, USA

<sup>e</sup> Institute of Paleobiology, Polish Academy of Sciences, Twarda 51/55, PL-00-818 Warsaw, Poland

<sup>f</sup> Yale University, Department of Geology and Geophysics, 210 Whitney Ave, New Haven, CT 06511, USA

<sup>g</sup> University of South Alabama, Department of Marine Sciences, Mobile, AL 36688, USA

<sup>h</sup> Dauphin Island Sea Lab, Dauphin Island, AL 36528, USA

Received 9 August 2018; accepted in revised form 30 January 2019; available online 6 February 2019

## Abstract

We measured U/Ca ratios, <sup>4</sup>He concentrations, <sup>234</sup>U/<sup>238</sup>U, and <sup>238</sup>U/<sup>235</sup>U in a subset of well-preserved aragonitic scleractinian fossil corals previously described by Gothmann et al. (2015). Comparisons of measured fossil coral He/U ages with the stratigraphic age demonstrate that well-preserved coral aragonite retains most or all of its radiogenic He for 10's of millions of years. Such samples must be largely or entirely free of alteration, including neomorphism. Measurements of <sup>234</sup>U/<sup>238</sup>U and <sup>238</sup>U/<sup>235</sup>U further help to characterize the fidelity with which the original U concentration has been preserved. Analyses of fossil coral U/Ca show that the seawater U/Ca ratio rose by a factor of 4–5 between the Early Cenozoic and today. Possible explanations for the observed increase include (1) the stabilization of U in seawater due to an increase in seawater [CO<sub>3</sub><sup>2-</sup>], and a resulting increase in UO<sub>2</sub>-CO<sub>3</sub> complexation as originally suggested by Broecker (1971); (2) a decrease in the rate of low-temperature hydrothermal alteration from Early Cenozoic to present, leading to a diminished U sink and higher seawater [U]; or (3) a decrease in uranium removal in reducing sediments, again leading to higher seawater [U].

© 2019 Elsevier Ltd. All rights reserved.

**Keywords:** Fossil coral; Seawater chemistry; Uranium isotopes; Cenozoic

## 1. INTRODUCTION

The geochemistry of uranium in seawater has long been of interest due to the use of uranium and its daughter isotopes as dating tools (Henderson and Anderson, 2003), and because of uranium's redox sensitive behavior

(Anderson, 1987; Barnes and Cochran, 1990; Morford and Emerson, 1999; Weyer et al., 2008). Uranium exists in seawater mainly as binary UO<sub>2</sub>-CO<sub>3</sub> and ternary Ca-UO<sub>2</sub>-CO<sub>3</sub> complexes (Langmuir, 1978; Djogic et al., 1986; Endrizzi and Rao, 2014; Endrizzi et al., 2016). The tendency for uranium to complex strongly with carbonate and with cations such as Ca dramatically increases its solubility (Langmuir, 1978; Bernhard et al., 2001; Dong and Brooks, 2006), leading to the conservative nature of uranium in seawater and its long residence time (3.5–5.6 × 10<sup>5</sup> yrs) (Chen

\* Corresponding author at: St. Olaf College, Departments of Environmental Studies and Physics, Northfield, MN 55057, USA.  
E-mail address: [gothmal@stolaf.edu](mailto:gothmal@stolaf.edu) (A.M. Gothmann).

et al., 1986). While U(VI) is present in well-oxygenated seawater, it is reduced to U(IV) in reducing sediments, rendering the uranium insoluble (Langmuir, 1978; Cochran et al., 1986; Anderson, 1987; Anderson et al., 1989). Experiments with Fe(III) and sulfate-reducing microorganisms indicate that this reduction is largely biologically-mediated (Lovley et al., 1991; Lovley and Phillips, 1992).

Despite interest in seawater uranium, the magnitudes of uranium fluxes to and from the modern ocean are poorly constrained (Table 1). Rivers are the principal source of uranium to seawater, and the dissolved uranium in rivers themselves is primarily derived from carbonate rocks and black shales (Palmer and Edmond, 1993). Additional sources of U include wind-blown dust and groundwater discharge, but the dust flux is likely minor in comparison with rivers, and the magnitude of the flux from groundwater discharge is not well known (Dunk et al., 2002; Henderson and Anderson, 2003; Tissot and Dauphas, 2015). The main seawater uranium sinks are uptake into suboxic sediments and low-temperature hydrothermal alteration of basalt (Barnes and Cochran, 1990; Klinkhammer and Palmer, 1991; Dunk et al., 2002; Henderson and Anderson, 2003; Mills and Dunk, 2010). Additional sinks include uptake in coastal

wetland sediments, uptake in anoxic sediments, high-temperature hydrothermal alteration, and co-precipitation with carbonate minerals and ferromanganese crusts (Barnes and Cochran, 1990; Klinkhammer and Palmer, 1991; Dunk et al., 2002; Wheat et al., 2003; Mills and Dunk, 2010). Although published estimates for the magnitudes of each source and sink terms exhibit a wide range ( $\sim \pm 50\%$  of fluxes; see Table 1), recent work using isotopic constraints on the seawater U budget suggest that the Dunk et al. (2002) estimates are likely the most reasonable (Tissot and Dauphas, 2015). This budget suggests that  $\sim 25\%$  of U is removed in suboxic sediments,  $\sim 23\%$  in marine carbonates,  $\sim 22\%$  in coastal sediments and Fe-Mn crusts,  $\sim 20\%$  in anoxic sediments, and  $\sim 10\%$  in altered basaltic crust.

The magnitudes of the uranium source and sink terms have likely changed relative to one another over multi-million-year timescales considering that they are closely linked with major geologic processes including continental weathering, ocean oxygenation, hydrothermal alteration, carbonate precipitation. Over the Cenozoic in particular, reconstructions of seawater Mg/Ca and Mg isotopes suggest that there may have been a decrease in low-temperature hydrothermal alteration rates between the

Table 1  
Summary of sources and sinks of seawater U.

	Flux (Mmol/yr)	Reference
<i>Sources of uranium to seawater:</i>		
Riverine	$42.0 \pm 14.5$	Dunk et al. (2002)
	36	Sarin et al. (1990)
	$45 \pm 15$	Palmer and Edmond (1993)
Submarine Groundwater	$9.3 \pm 8.7$	Dunk et al. (2002)
Aeolian	$1.8 \pm 1.1$	Dunk et al. (2002)
Total	$53.1 \pm 16.9$	Dunk et al. (2002)
<i>Sinks for uranium from seawater:</i>		
Suboxic sediments	$15.3 \pm 10.6$	Dunk et al. (2002)
	28	Klinkhammer and Palmer (1991)
	12	Barnes and Cochran (1990)
Coastal zone sediments	$11.2 \pm 5.6$	Dunk et al. (2002)
Basalt alteration <sup>a</sup>	$5.7 \pm 3.3$	Dunk et al. (2002)
	$16 \pm 4$	Palmer and Edmond (1989) <sup>1</sup>
	7.4	Wheat et al. (2003) <sup>2</sup>
	$11.2 \pm 17.8$	Mills and Dunk (2010)
	$12.5 \pm 2.5$	James et al. (2003)
	$19 \pm 7$	Morford and Emerson (1999) <sup>3</sup>
Anoxic sediments	$11.6 \pm 6.0$	Dunk et al. (2002)
Carbonate sediments	$13.3 \pm 5.6$	Dunk et al. (2002) <sup>4</sup>
	3.4	Cochran (1982) <sup>5</sup>
metalliferous sediment	$1.0 \pm 0.8$	Dunk et al. (2002)
Total	$58.1 \pm 14.9$	Dunk et al. (2002)

<sup>1</sup> Assuming high-T hydrothermal water fluxes calculated from the seawater  $^{87}\text{Sr}/^{86}\text{Sr}$  budget and quantitative consumption of U during high-T basalt alteration.

<sup>2</sup> Assuming a river U flux of 32 Mmol/yr.

<sup>3</sup> Compiled from estimates made by Chen et al. (1986) and Hart and Staudigel (1982).

<sup>4</sup> Using the shallow water carbonate budget of Milliman (1993).

<sup>5</sup> Also used for Barnes and Cochran (1990) and Morford and Emerson (1999) U budgets.

<sup>a</sup> The basalt alteration fluxes here include total estimates considering both low-T and high-T alteration of basalt, but whereas low-T basalt alteration is associated with an isotopic fractionation, high-T basalt alteration is quantitative with no isotopic fractionation (see Tissot and Dauphas, 2015 for a recent discussion).

early Cenozoic and today or, alternatively, a decrease in silicate weathering rates (e.g., Higgins and Schrag, 2015; Gothmann et al., 2015; 2017). Changes in these processes could affect seawater uranium abundances as well, since rivers are the main seawater source and low-temperature hydrothermal alteration is a major uranium sink (e.g. Dunk et al., 2002).

Seawater uranium abundances may also be sensitive to changes in uranium speciation, which are expected to result from changes in Cenozoic ocean carbonate chemistry and major ion composition (e.g., Lowenstein et al., 2003; Tyrrell and Zeebe, 2004; Höönicke et al., 2012; Zeebe, 2012; Hain et al., 2015). Specifically, Chen et al. (2017) calculate that the most abundant uranium complex in modern seawater ( $\text{Ca}_2\text{UO}_2(\text{CO}_3)_3$  (aq)) may have decreased in abundance relative to total uranium by ~30% between the early Cenozoic and today. While changes in speciation alone should not affect the total concentration of dissolved uranium in seawater, experimental evidence suggests that uranium removal rates from seawater may depend on uranium speciation (Wazne et al., 2003; Hua et al., 2006; Belli et al., 2015; DeCarlo et al., 2015).

Finally, uranium abundances and isotopic composition in seawater may be sensitive to changes in ocean oxygenation. Recently published  $\delta^{238/235}\text{U}$  records provide some constraints on variations in the anoxic uranium sink over the Cenozoic (Goto et al., 2014; Wang et al., 2016a).  $^{238}\text{U}/^{235}\text{U}$  varies in nature due to a mass-independent “nuclear volume” isotope effect. Specifically, the heavy isotopes of uranium (those with larger nuclear volumes) are more abundant in U(IV) relative to U(VI) phases, given that reduced U has a lower number of s orbital electrons and thus a lower electron density at the nucleus (e.g. Bigeleisen, 1996; Schable, 2007). This isotope effect has been observed in experiments where uranium has been reduced both by biological and abiotic means (Basu et al., 2014; Stylo et al., 2015; Stirling et al., 2015; Brown et al., 2018). Thus, reconstructions of seawater  $\delta^{238/235}\text{U}$  can track the relative importance of uranium removal by reduction relative to other sinks (e.g., Weyer et al., 2008; Montoya-Pino et al., 2010; Brennecke et al., 2011; Kendall et al., 2013).

In this paper, we present data on U/Ca,  $^{234}\text{U}/^{238}\text{U}$ ,  $^{238}\text{U}/^{235}\text{U}$ , and  $^4\text{He}$  concentrations (hence  $^4\text{He}/\text{U}$  ages) from a set of well preserved aragonitic fossil corals with ages ranging from modern to Jurassic. The coral U partition coefficient ( $K_{\text{U/Ca,sw-coral}}^{\text{D}} = [\text{U}/\text{Ca}_{\text{coral}}]/[\text{U}/\text{Ca}_{\text{seawater}}]$ ) is close to 1 and culture experiments have demonstrated that coral U/Ca increases linearly with increasing seawater [U] (Broecker, 1971; Swart and Hubbard, 1982; Thompson et al., 2003; Robinson et al., 2006). In addition, spectroscopic studies (XAFS) indicate that uranium is likely incorporated in the aragonite lattice from seawater without undergoing a coordination change and is structurally stable (Reeder et al., 2000). As long as primary aragonite has not recrystallized to calcite, these findings suggest that uranium uptake in aragonite is less likely to be discriminated against and also that uranium in aragonite may be preserved over long timescales. As a result, it is possible that fossil corals can capture variations in seawater U/Ca.

Our fossil coral sample set has been screened for diagenesis using x-ray diffractometry, scanning electron microscopy, petrographic microscopy, cathodoluminescence microscopy, micro-raman spectroscopy,  $^{87}\text{Sr}/^{86}\text{Sr}$  measurements, carbonate clumped isotope thermometry, and Secondary Ion Mass Spectrometry (SIMS) measurements of trace elements (Gothmann et al., 2015). As reported in this paper, fossil coral uranium integrity is evaluated further by  $^4\text{He}/\text{U}$  ages as well as measurements of U isotopes ( $^{234}\text{U}/^{238}\text{U}$ ,  $^{238}\text{U}/^{235}\text{U}$ ). Measurements of fossil coral U/Ca indicate a factor of 4–5 increase between the early Cenozoic and today that we attribute to an increase in seawater U/Ca. We evaluate the potential for a range of geologic processes important for elemental cycling to drive the observed changes in Cenozoic fossil coral U/Ca, including changes in uranium river flux, changes in uranium solubility in seawater, changes in uranium removal during low-temperature hydrothermal alteration and changes in uranium removal in reducing sediments. While it is not possible to determine which of these processes is likely to be most important, the U/Ca data allow us to place bounds on variations in the fluxes examined.

## 2. METHODS

### 2.1. U/Ca measurements

For full details regarding fossil sample identification, provenance, and ages, the reader is referred to the [supplementary materials](#). Small pieces of coral skeleton were cut using a dremel tool and crushed into ~1 mm pieces using a mortar and pestle. Aliquots of approximately 10 mg, corresponding to ~20 chunks of coral aragonite for each aliquot, were dissolved in 1 N nitric acid ( $\text{HNO}_3$ ) for U/Ca analyses. Dissolved samples were centrifuged, inspected for insoluble residues, and diluted to a concentration of 60 ppm Ca in preparation for mass spectrometry. U/Ca measurements were conducted using a Thermo Finnigan Element-2 Inductively Coupled Plasma Mass Spectrometer (ICP-MS) at Princeton University. Ratios were calibrated using a set of matrix-matched in-house standards with U/Ca ratios spanning our sample range as in Rosenthal et al. (1999). The external reproducibility of an in-house deep-sea coral standard prepared the same way as coral samples was ~6%  $2\sigma$  s.d. (where s.d. is standard deviation).

### 2.2. $^4\text{He}$ measurements and He/U calculation

Additional ~10 mg aliquots were weighed and wrapped in foil in preparation for He extraction. Samples were loaded into a vacuum furnace and heated to 1200 °C to degas He. The evolved gas was then purified cryogenically and inlet to a MAP 215-50 noble gas mass spectrometer at the California Institute of Technology to measure  $^4\text{He}$  concentrations. Sensitivity was calibrated through frequent measurements of air standards run at  $^4\text{He}$  concentrations spanning the expected range of our samples. The reproducibility of standards run throughout the analysis session was <1%  $2\sigma$  s.d. for  $^4\text{He}$ . Hot blanks, line blanks, and sample re-extracts were run routinely throughout the analysis

session, and re-extracts were always at or below hot blank values, suggesting that all sample  ${}^4\text{He}$  was extracted from the sample during analysis. Both the hot blanks and re-extracts are reflective of our instrument blank, and we use these data to blank-correct all samples. We attribute an uncertainty of 0.1 ncc  ${}^4\text{He}$  to this blank correction.

### 2.3. Uranium isotope analyses

A subset of samples was analyzed for both  ${}^{234}\text{U}/{}^{238}\text{U}$  and  ${}^{238}\text{U}/{}^{235}\text{U}$  ratios. Approximately 50 mg of coral were required for these measurements, and so we were limited to analyzing samples with sufficient material. Multiple chunks of coral sample  $\sim 1$  mm in size were powdered using a mortar and pestle in preparation for uranium isotope analyses. Using estimates of coral [U] from U/Ca measurements, coral powders corresponding to 50–100 ng U were weighed and dissolved in 10 mL of 0.5 N  $\text{HNO}_3$ . These samples were centrifuged and the supernatant was poured off to avoid small amounts of organics and/or insoluble silicate residue. Sample U was separated from matrix as described in Wang et al. (2016a). Briefly, samples were spiked with 25–50  $\mu\text{L}$  of an in-house  ${}^{233}\text{U}$ - ${}^{236}\text{U}$  double-spike to achieve a  ${}^{238}\text{U}/{}^{236}\text{U}$  ratio of  $\sim 30$ . The spiked samples were dried and re-dissolved in 3 N  $\text{HNO}_3$  in preparation for uranium purification. Uranium was separated by eluting through a column filled with Eichrom UTEVA (100–150  $\mu\text{m}$ ) resin. After eluting the matrix using 3 N  $\text{HNO}_3$ , Th was eluted in two steps using 10 N HCl and 5 N HCl, and finally U was eluted and collected with 0.05 N HCl. Purified U samples were dried down once more, treated with concentrated  $\text{HNO}_3$  at 130 °C to remove potential organic matter leached from the resin, and finally dissolved in 0.75 N  $\text{HNO}_3$  at  $\sim 50$  ppb U with 5%  $\text{HNO}_3$  in preparation for mass spectrometry.

Measurements were conducted at Yale University using a Thermo Scientific Neptune Plus multicollector inductively coupled mass spectrometer (MC-ICP-MS) with an ESI Apex-IR sample introduction system (see Wang et al., 2016a for details). Baseline measurements and gain calibrations were performed prior to every analytical session. Beam intensities for  ${}^{232}\text{Th}$ ,  ${}^{233}\text{U}$ ,  ${}^{234}\text{U}$ ,  ${}^{235}\text{U}$ ,  ${}^{236}\text{U}$ , and  ${}^{238}\text{U}$  were concurrently measured in low resolution using Faraday collectors. All isotopes were collected using  $10^{11} \Omega$  resistors with the exception of  ${}^{238}\text{U}$ , for which a  $10^{10} \Omega$  resistor was used, and  ${}^{235}\text{U}$ , for which a  $10^{12} \Omega$  resistor was used. Sensitivity for  ${}^{238}\text{U}$  was  $\sim 35$  V for a 50 ppb solution. Data were acquired in 5 blocks of 10 cycles each, with 4.19 s integration per cycle. Instrumental mass bias was accounted for using the  ${}^{233}\text{U}$ - ${}^{236}\text{U}$  double-spike.  ${}^{238}\text{U}/{}^{235}\text{U}$  are reported as  $\delta^{238/235}\text{U}$  relative to the composition of the U metal standard CRM112a, measured during the same analytical session. One CRM112a standard was measured for every 3 samples. Procedural blanks were  $\sim 10$ –40 pg which was  $<0.05\%$  of the sample U content. In addition to samples, we measured a USGS Fe-Mn crust standard (Nod-A-1) taken through the entire chemical procedure, to assess the accuracy and long-term reproducibility of the method. For Nod-A-1, we measured a value of  $\delta^{238/235}\text{U} = -0.59 \pm 0.10\%$  ( $2\sigma$  s.d.), and  $\{{}^{234}\text{U}/{}^{238}\text{U}\}$

$= 1.087 \pm 0.030$  ( $2\sigma$  s.d.);  $n = 7$ . For BHVO-2, a basalt standard, we measured a composition of  $\delta^{238/235}\text{U} = -0.26 \pm 0.12\%$  ( $2\sigma$  s.d.), and  $\{{}^{234}\text{U}/{}^{238}\text{U}\} = 0.997 \pm 0.032$  ( $2\sigma$  s.d.);  $n = 12$ . The average measured isotopic compositions for standards are consistent with values published previously (Weyer et al., 2008; Tissot and Dauphas, 2015; Wang et al., 2016a).

## 3. RESULTS AND DISCUSSION

### 3.1. He/U dating of fossil corals

After formation of coral aragonite,  ${}^{238}\text{U}$  and  ${}^{235}\text{U}$  present in coral skeletons decay to their lead daughters ( ${}^{206}\text{Pb}$  and  ${}^{207}\text{Pb}$ ) producing  ${}^4\text{He}$  through alpha-decay (described below in Eq. (1)).

$$[{}^4\text{He}] = 8[{}^{238}\text{U}](e^{2238t} - 1) + 7[{}^{235}\text{U}](e^{2235t} - 1) + 6[{}^{232}\text{Th}](e^{2232t} - 1), \quad (1)$$

Because negligible amounts of Th are incorporated in clean coral carbonate, the third term in Eq. (1) above can be ignored (Bender, 1973; Thompson et al., 2003). Using measured uranium and  ${}^4\text{He}$  concentrations, it is possible to use Eq. (1) to solve for the age of the sample,  $t$ . Previous studies have shown that  $\sim 70$ –100% of radiogenic  ${}^4\text{He}$  produced by uranium decay is retained in well preserved fossil corals (Fanale and Schaeffer, 1965; Bender, 1973). For one sample presented here that is younger than  $\sim 1$  Myr, uranium daughters are not yet at secular equilibrium and so He production is a more complicated function of time. We apply the equations presented in Bender (1973) to calculate He/U ages for this single sample.

Because coral skeletons have intricate physical structures and fine ( $\sim 10$ –1000  $\mu\text{m}$  scale) intersecting features, it is necessary to correct calculated He/U ages for He-loss associated with alpha particle ejection from coral aragonite (Bender, 1973; Farley et al., 1996). In Bender's (1973) sample suite, alpha ejection losses as high as 20–30% were calculated from the geometry of some samples. This amount of loss is due to similarities in magnitude between the distance that emitted alpha particles can travel for aragonite (20  $\mu\text{m}$ ; Schroeder et al., 1970; Bender, 1973) and the width of some features of the coral skeleton (Schroeder et al., 1970; Roniewicz and Stolarski, 1999). Assuming a homogeneous uranium distribution in the skeleton, Bender (1973) calculated the fraction ( $F$ ) of  ${}^4\text{He}$  that should be lost for a given thickness of coral skeleton. Here we estimate this  $F$ -value for our samples based on their skeletal geometry in an effort to correct for alpha ejection as in Bender (1973) (Table 2). This correction factor has a large uncertainty for two reasons: (1) our treatment of the geometry of the coral skeleton is oversimplified, and (2) the assumption of homogeneous [U] in the coral skeleton is inaccurate (see, for example, Robinson et al., 2006). For this reason, we assign  $\pm 20\%$  uncertainty to our estimated  $F$ -values. Not all of the samples studied here require a He-loss correction because we were sometimes able to sample dense, massive (non-porous) skeletal material from the base of the coral calyx (i.e. the bottom-most part of the coral skeleton). In

Table 2

Summary of U/Ca results, He/U dating experiments, and alpha ejection correction calculations. Alpha ejection correction calculations are after Bender (1973). Samples for which the correction was not applied were massive (see [supplementary Fig. S1](#)), and so the magnitude of He loss from alpha ejection is assumed to be insignificant. Expected ages of the samples are from Gothmann et al. (2015) from stratigraphic constraints or measurements of  $^{87}\text{Sr}/^{86}\text{Sr}$  ratios. The column labeled 'zoox/azoox' notes best estimates for whether fossil coral samples are zooxanthellate (symbiotic) or azooxanthellate (asymbiotic). Fossil specimens for which modern analogues can be either symbiotic or asymbiotic are marked 'nk'. Estimates come from consideration of species identifications (for more information see [supplementary Table S1](#)) and examinations of skeletal structure and morphology.

ID	Expected Age (Ma)	Expected Age Uncertainty (Ma)	$^{87}\text{Sr}/^{86}\text{Sr}$ (Gothmann et al., 2015)	U/Ca ( $\mu\text{mol/mol}$ )	2 $\sigma$ s.d.	$^4\text{He}$ (ncc/g $\text{CaCO}_3$ )	2 $\sigma$ s.d.	Un-corrected He Age (Myr)	2 $\sigma$ r.s.	F <sup>a</sup>	I <sup>b</sup>	Corrected He Age (Myr)	2 $\sigma$ s.d. <sup>c</sup>	zoox/azoox not known	Notes
RSCL901	0	0	—	1.19	0.07	—	—	—	—	—	—	—	—	—	
RSCL909	0	0	—	0.98	0.06	—	—	—	—	—	—	—	—	—	
Pl3	0.1	0.05	—	1.14	—	105	7	0.38	9	0.25	0.1	0.49	0.04	zoox	Porous
Pl2	1.4	0.05	0.709113	0.86	0.03	289	11	1.2	7	—	—	1.20	0.08	azoox	Massive
Pl8	2.2	0.09	0.709078	1.08	0.11	541	8	1.85	6	0.15	0.01	2.17	0.13	azoox	Porous
Pl7	2.3	0.06	0.709076	1.42	0.1	669	8	1.72	6	0.25	0.01	2.29	0.14	zoox	Porous
Pl3	2.3	0.08	0.709075	1.04	0.03	764	10	2.58	6.5	0.2	0.1	3.15	0.20	azoox	Porous
Pl1	3.5	1	—	0.62	0	932	12	5.38	6	—	—	5.38	0.32	azoox	Massive
Pl2	3.8	0.35	0.709055	1	—	951	12	3.06	6	0.2	0.1	3.73	0.22	nk	Porous
Mi6	5.4	0.07	0.709023	0.66	0	871	11	4.7	6	0.2	0.01	5.86	0.35	zoox	Porous
Mi11	9.3	2	—	1.15	0.22	1606	12	5.32	6	0.1	0.01	5.90	0.35	zoox	Porous
Mi13	9.4	0.23	0.708908	0.58	—	1512	10	7.97	6	0.2	0.01	9.94	0.60	zoox	Porous
Mi7	14	0.59	0.708802	0.8	0	2637	227	13.2	10	0.02	0.01	13.47	1.35	azoox	Some pore space
Mi8	14	9	—	0.96	—	5916	4425	22.3	78	0.12	0.01	25.31	19.74	zoox	Silicate residue
Mi2	17.8	0.08	0.708602	0.48	0.01	1958	73	14.2	7	0.2	0.01	17.71	1.24	zoox	Porous
Mi1	18	0.14	0.708601	0.33	0.04	1696	12	17.2	6	—	—	17.20	1.03	zoox	Massive
Mi3	18.2	0.13	0.708577	0.6	0.06	3005	965	17.4	32	0.08	0.01	18.90	6.05	zoox	Some pore space/some silicate residue
Ol3	31.8	0.51	0.70791	0.34	—	2753	11	24.8	6	0.02	0.01	25.30	1.52	nk	Some pore space
Ol4	32.4	0.13	0.707895	0.27	0.06	2015	11	24.5	6	0.02	0.01	24.99	1.50	zoox	Some pore space
Ol6	30	0.13	—	0.29	0.04	2498	11	28.3	6	0.02	0.01	28.87	1.73	zoox	Some pore space
Ol5	32.6	0.17	0.707889	0.22	0.06	2062	121	31	8	0.02	0.1	31.57	2.53	zoox	Some pore space
E6	35	0.48	0.707889	0.81	0.03	5131	303	20.2	9	0.3	0.01	28.73	2.59	zoox	Porous
E8	37	0.63	0.707748	0.24	—	3012	11	38	6	—	—	38.00	2.28	azoox	Massive/some silicate residue
Ol2	37.7	0.83	0.707742	0.25	—	2556	11	28.4	6	0.02	0.01	28.97	1.74	azoox	Some pore space
E1	39.2	0.5	0.707718	0.38	0.04	3758	611	33.3	17	0.1	0.01	36.96	6.28	azoox	Half porous/massive
E7	48.9	10	0.707715	0.13	—	1262	9	30.2	6	—	—	30.20	1.81	zoox	Massive, 35% calcite in powder
E3	41	9.03	0.707744	0.37	0.02	3022	287	28	11	0.08	0.01	30.41	3.34	azoox	Some pore space
E5	39.9	10.13	0.707767	0.26	0.05	3614	56	45.6	7	0.1	0.01	50.61	3.54	zoox	Porous
E4	46.7	6.68	0.707735	0.3	0.02	3497	12	40.2	6	0.02	0.01	41.01	2.46	azoox	Some pore space
Pa1	60	4	—	0.49	0	11,019	392	74.1	7	—	—	74.10	5.19	azoox	Massive/some silicate residue
Pa3	60.1	1.68	0.707805	0.45	0.01	8216	261	62.3	6	0.02	0.01	63.56	3.81	azoox	Some pore space
K2	86.7	0.05	0.707403	0.14	—	2919	35	54.5	6	—	—	54.50	3.27	zoox	Massive, 15% calcite in powder
J1	160.3	0.08	0.706844	0.44	0.1	16,467	206	137.3	6	0.12	0.01	155.81	9.35	zoox	Porous
J4	161.5	0.38	0.706861	0.56	—	20,753	17	127.1	6	0.15	0.01	149.27	8.96	zoox	Porous

<sup>a</sup> F is based on coral skeleton thickness and is assigned an uncertainty of  $\pm 20\%$ .

<sup>b</sup> I is based on the number of intersections between different coral skeleton components.

<sup>c</sup> 2 $\sigma$  s.d. for corrected He ages are calculated by propagating uncertainty from replicate He analyses, U concentrations (6% based on repeat analyses of coral standard) and from the uncertainty associated with the alpha-loss correction.

addition to specifying a value for  $F$ , Bender used an ‘intersection correction’ ( $I$ ), corresponding to the point of connection between intersecting features of the coral skeleton (for example the intersection point between a coral septum and the coral thecal wall). These intersections decrease the percentage of  ${}^4\text{He}$  lost. We give values for  $I$  in Table 2 as well.

We calculate the corrected  ${}^4\text{He}$  age from Eq. (1) above using an adjusted uranium concentration:

$$\text{Adjusted } [\text{U}] = \text{Measured } [\text{U}] \times [1 - F \times (1 - I)]. \quad (2)$$

The adjusted U concentration discounts the measured U concentration by the fraction of He lost due to recoil. Fig. 1 shows our calculated, corrected He/U ages for samples plotted against the expected age of the sample from biostratigraphic constraints and Sr isotope measurements (Gothmann et al., 2015). Fig. 2 shows a second comparison of our He/U ages relative to the expected age of the sample, where samples are plotted on the MacArthur et al. (2001) Sr isotope curve. Both Figs. 1 and 2 demonstrate that the majority, but not all, of fossil coral samples analyzed agree with the expected age to within uncertainty. Samples with He/U ages younger than the expected stratigraphic age ( $n = 9$ ) may indicate yet-unrecognized alteration – specifically, addition of diagenetic  ${}^{238}\text{U}$  and  ${}^{235}\text{U}$ . Fossil coral samples that give He-ages older than expected ( $n = 5$ ) may result from He implantation due to infilling clay-rich muds or sediment. Alternatively, this He may derive from the decay of Th adsorbed onto the surface of the skeleton throughout the coral’s existence (Cheng et al., 2000; Thompson et al., 2003; Robinson et al., 2006). He implan-

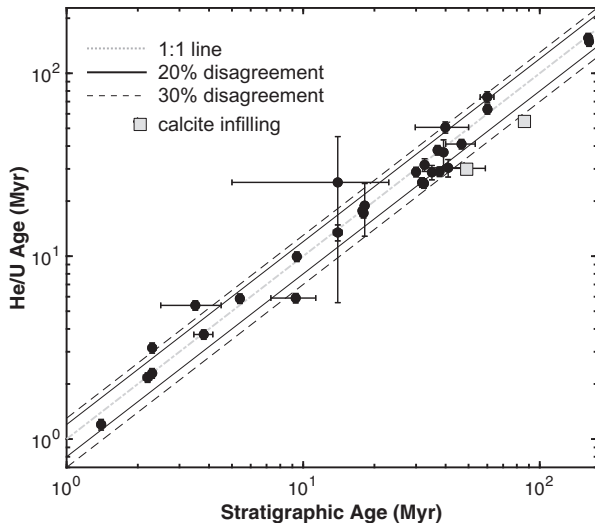


Fig. 1. Corrected He/U ages vs. independently constrained age (Myr). Independent ages are from radiogenic Sr isotope measurements or from biostratigraphic constraints on the age of the geologic formation from which fossil coral samples were collected (Table 2; Gothmann et al., 2015). Grey squares correspond to samples that are excluded from our U/Ca record due to the presence of calcite in drilled powders. Y-axis error bars correspond to propagated uncertainty from replicate errors in  ${}^4\text{He}$  and U/Ca analyses, and uncertainty due to the  $F$ -value correction. X-axis error bars correspond to uncertainties in the stratigraphic age.

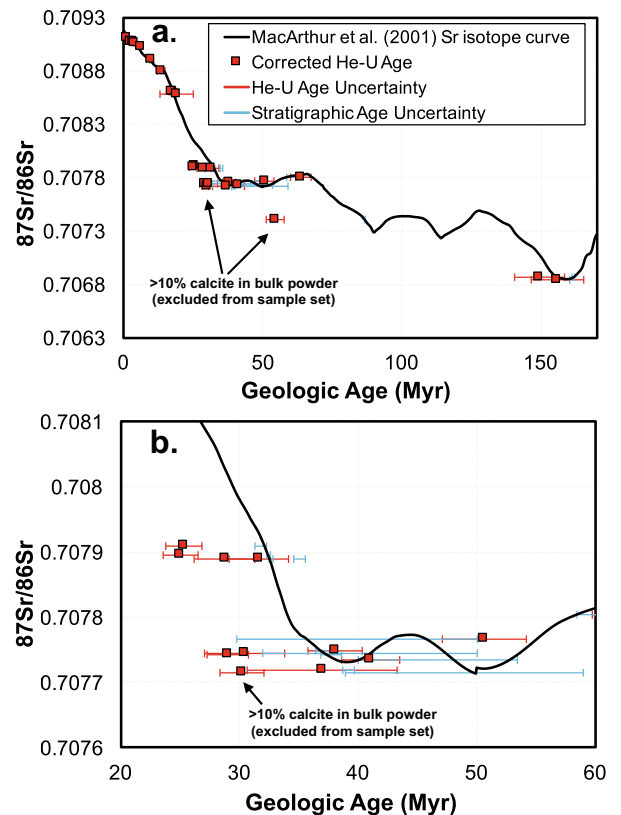


Fig. 2. (a) Comparison of calculated He/U ages and  ${}^{87}\text{Sr}/{}^{86}\text{Sr}$  ratios measured on the same sample set as reported in Gothmann et al. (2015). Calculated He/U ages are corrected for He-loss as described in Section 3.1. Error bars shown in red correspond to the  $2\sigma$  s.d. uncertainties on corrected He/U ages (see Table 2). (b) Enlarged version of (a) from 20 to 60 Ma.

tation and decay of adsorbed Th should only affect the He-age (and not the coral U/Ca ratio). The existence of multiple diffusion domains, which can occur if there are a range of crystal sizes present within a mineral, and micro-cracks have been suggested to be important for He-loss in calcite (Copeland et al., 2007; Cros et al., 2014; Amidon et al., 2015; Cherniak et al., 2015). The presence of such features might also account for some of the variability in He-loss from one sample to another.

We also measured two samples containing a mixture of coral skeleton and secondary cement infilling as inferred from x-ray diffraction. These samples give He-ages that are  $\sim 30\%$  younger than the expected age (see grey squares in Fig. 1 and notes in Table 2) and are also characterized by relatively low U/Ca ratios. Because our He/U age is not lower than the expected stratigraphic age by more than 30%, we interpret this result as indicating good preservation of the original coral skeleton combined with a minor U contribution from the secondary cement. In other words, if our sample is a mixture of primary aragonite (with high U/Ca and high  $[{}^4\text{He}]$ ) and secondary calcite (with low U/Ca and low  $[{}^4\text{He}]$ ), then the He/U age would largely reflect the composition of the primary aragonite.

Our He/U analyses provide constraints on the preservation of U in our fossil coral samples. We flag fossil coral

samples with He/U ages that underestimate the expected age beyond uncertainty due to the possibility that these offsets indicate the presence of a diagenetic component. As stated above, because ages that are too-old are likely caused by processes that affect He production instead of processes that alter U/Ca ratios, we do not reject these samples. Table 3 lists all geochemical criteria from this study used to flag or exclude samples.

### 3.2. $^{234}\text{U}/^{238}\text{U}$ and $\delta^{238/235}\text{U}$ compositions of fossil corals

#### 3.2.1. $^{234}\text{U}/^{238}\text{U}$

The modern seawater activity ratio of  $^{234}\text{U}$  and  $^{238}\text{U}$ , denoted as  $\{\text{U}/^{238}\text{U}\}$ , is enriched in  $^{234}\text{U}$  ( $\{\text{U}/^{238}\text{U}\} = 1.1468$ ; Andersen et al., 2010) relative to secular equilibrium ( $\{\text{U}/^{238}\text{U}\} = 1$ ). This can be explained by  $\alpha$ -recoil

of  $^{234}\text{U}$  from minerals on land, and diffusion of  $^{234}\text{U}$  (again liberated by  $\alpha$ -recoil) from oceanic sediments through pore waters into seawater (Ku, 1965; Chen et al., 1986; Cheng et al., 2000; Henderson and Anderson, 2003; Pogge von Strandmann et al., 2010). We expect modern coral  $\{\text{U}/^{238}\text{U}\}$  to be within error of the modern seawater value. Although recent studies suggest that seawater  $\{\text{U}/^{238}\text{U}\}$  has varied over glacial-interglacial timescales (e.g., Esat and Yokoyama, 2006; Chutcharavan et al., 2018; Tissot et al., 2018), almost all fossil corals studied here have geologic ages  $>1$  Ma. Because the decay constant for  $^{234}\text{U}$  is large compared with the decay constant for  $^{238}\text{U}$  (its ultimate source), the activity ratio of  $^{234}\text{U}$  to  $^{238}\text{U}$  in corals approaches secular equilibrium after  $\sim 1$  Ma (assuming closed system behavior). Measured  $\{\text{U}/^{238}\text{U}\}$  ratios greater or less than one for our fossil corals should there-

Table 3

Summary of criteria for flagging/excluding samples from U/Ca record based on He/U ages and U isotopes. Cells marked with an 'x' indicate that a sample meets the criterion described in the column header. Samples not analyzed for He/U or U isotopes are marked 'n.a.'

ID	Age (Ma)	U/Ca ( $\mu\text{mol/mol}$ )	He/U Age underestimates expected age beyond uncertainty	$\{\text{U}/^{238}\text{U}\}$ is $> 0.03$ offset from secular equilibrium*	$\delta^{238/235}\text{U}$ is $> 0.10$ (permil) offset from modern coral average**	Presence of calcite in bulk powder	Assessment (e = excluded, f = flagged)
RSCL890	0	1.43	n.a.				
RSCL894	0	1.16	n.a.				
RSCL899	0	1.03	n.a.				
RSCL901	0	1.19	n.a.				
RSCL909	0	0.98	n.a.				
Pl3	0.1	1.14		n.a.	n.a.		
Pl2	1.4	0.86	x				f
Pl8	2.2	1.08		x			f
Pl7	2.3	1.42		x			f
Pli3	2.3	1.04					
Pli1	3.5	0.62		n.a.	n.a.		
Pli2	3.8	1.00		x	x		f
Mi6	5.4	0.66					
Mi11	9.3	1.15	x	x	x		f
Mi13	9.4	0.58			x		f
Mi7	14	0.80		n.a.	n.a.		
Mi8	14	0.96		n.a.	n.a.		
Mi2	17.8	0.48			x		f
Mi1	18	0.33		x			f
Mi3	18.2	0.60					
Ol3	31.8	0.34	x	n.a.	n.a.		f
Ol4	32.4	0.27	x				f
Ol6	30	0.29		n.a.	n.a.		
Ol5	32.6	0.22		n.a.	n.a.		
E6	35	0.81	x	x	x		f
E8	37	0.24					
Ol2	37.7	0.25	x	n.a.	n.a.		f
E1	39.2	0.38		n.a.	n.a.		
E7	48.9	0.13	x	n.a.	n.a.	x	e
E3	41	0.37		n.a.	n.a.		
E5	39.9	0.26		x			f
E4	46.7	0.30					
Pa1	60	0.49		n.a.	n.a.		
Pa3	60.1	0.45		n.a.	n.a.		
K2	86.7	0.14	x	n.a.	n.a.	x	e
J1	160.3	0.44		n.a.	n.a.		
J4	161.5	0.56	x	n.a.	n.a.		f

\* Offset criterion for  $\{\text{U}/^{238}\text{U}\}$  is based on the external precision of the Nod-A-1 basalt standard ( $\pm 0.03 2\sigma$  s.d.).

\*\* Offset criterion for  $\delta^{238/235}\text{U}$  is based on the external precision of the Nod-A-1 standard ( $\pm 0.1 2\sigma$  s.d.).

fore indicate post-depositional alteration of primary U and we can use  $\{\text{<sup>234</sup>U}/\text{<sup>238</sup>U}\}$  in our fossil corals as an additional constraint on preservation. More specifically, higher  $\{\text{<sup>234</sup>U}/\text{<sup>238</sup>U}\}$  could indicate addition of U, for example from groundwaters. Alternatively, lower  $\{\text{<sup>234</sup>U}/\text{<sup>238</sup>U}\}$  might indicate  $\alpha$ -recoil loss of  $\text{<sup>234</sup>U}$  from our samples.

**Fig. 3a** and **Table S2** show results of  $\{\text{<sup>234</sup>U}/\text{<sup>238</sup>U}\}$  measurements. Modern samples show values consistent with the known activity ratio of modern seawater. Samples younger than  $\sim 1$  Ma are enriched in  $\text{<sup>234</sup>U}/\text{<sup>238</sup>U}$  as is expected based on the modern seawater ratio. Of our samples older than 1 Ma, there are 7 fossil samples that deviate from secular equilibrium beyond the external reproducibility of our measured Nod-A-1 standard (see **Section 2.3**). Two of these fossil coral samples have  $\{\text{<sup>234</sup>U}/\text{<sup>238</sup>U}\}$  ratios even higher than that of modern seawater  $\{\text{<sup>234</sup>U}/\text{<sup>238</sup>U}\}$  (**Table S2**). Although these samples do not have visibly higher [U] from samples of similar geologic age, we flag them in our U/Ca record. The most likely explanation for the high  $\{\text{<sup>234</sup>U}/\text{<sup>238</sup>U}\}$  values observed in such samples is that  $\text{<sup>234</sup>Th}$  from groundwaters, which decays to  $\text{<sup>234</sup>U}$ , is added by absorption (Thompson et al., 2003). The absorbed  $\text{<sup>234</sup>Th}$  component may enhance He production rates, and thus  ${}^4\text{He}/\text{U}$  ages, by only a few percent. Indeed, there is no clear relationship between  $\{\text{<sup>234</sup>U}/\text{<sup>238</sup>U}\}$  and U/Ca, or between  $\{\text{<sup>234</sup>U}/\text{<sup>238</sup>U}\}$  and the relative deviation in He-U age from expected age for fossil samples greater than 1 Ma (see **supplementary Figs. S2 and S3**).

### 3.2.2. $\delta^{238}/\text{<sup>235</sup>U}$

Modern seawater has a  $\delta^{238}/\text{<sup>235</sup>U}$  composition of  $-0.392 \pm 0.005\text{\textperthousand}$  (Stirling et al., 2007; Weyer et al., 2008; Tissot and Dauphas, 2015). Published measurements of modern coral  $\delta^{238}/\text{<sup>235</sup>U}$  span a range of values:  $\sim -0.37$

to  $-0.5\text{\textperthousand}$  with an average of  $-0.39 \pm 0.06\text{\textperthousand}$  ( $2\sigma$  s.d.) (Stirling et al., 2007; Weyer et al., 2008; Tissot and Dauphas, 2015; Chen et al., 2018a; Chen et al., 2018b; Tissot et al., 2018). The most recent, high precision measurements of coral  $\delta^{238}/\text{<sup>235</sup>U}$  ( $n = 11$ ) yield an average of  $-0.37 \pm 0.02\text{\textperthousand}$  ( $2\sigma$  s.d.) (Chen et al., 2018a; Chen et al., 2018b; Tissot et al., 2018). Modern corals measured in this study ( $n = 5$ ) are consistent with previous measurements with an average of  $-0.36 \pm 0.06\text{\textperthousand}$  ( $2\sigma$  s.d.). The similarity between coral and seawater  $\delta^{238}/\text{<sup>235</sup>U}$  has been interpreted to reflect equilibrium isotope fractionation between uranium species during inorganic aragonite precipitation coupled with biological vital effects associated with coral calcification (Chen et al., 2016; 2017; 2018a). Specifically, carbonate precipitation experiments show that inorganic aragonite has a  $\delta^{238}/\text{<sup>235</sup>U}$  that is  $0.11\text{\textperthousand}$  heavier than seawater consistent with  $\text{<sup>238</sup>U}$  being preferentially incorporated into inorganic aragonite under conditions where the abundance of the neutral  $\text{Ca}_2\text{UO}_2(\text{CO}_3)_3$  aqueous species is greater (Chen et al., 2016; 2017). The observation that coral  $\delta^{238}/\text{<sup>235</sup>U}$  is not as isotopically heavy as inorganic aragonite could suggest the presence of reservoir effects or precipitation rate effects at the site of coral calcification (Chen et al., 2018a). It has recently been shown that  $\delta^{238}/\text{<sup>235</sup>U}$  may vary on a fine scale in coral as a result in compositional differences between the centers of calcification (COCs, associated with rapid calcification and small crystal size) and coral fibers (associated with slower calcification and larger grain size) (Tissot et al., 2018). Our bulk sampling should largely minimize heterogeneity in coral  $\delta^{238}/\text{<sup>235</sup>U}$  that could arise from such differences, but we do not have quantitative constraints on the exact proportions of COC and fibers within each sample.

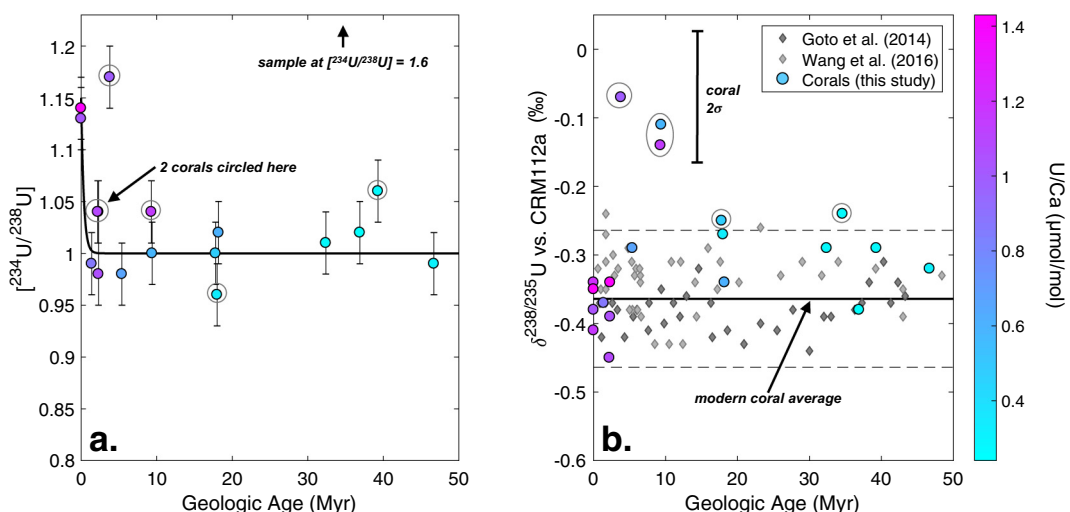


**Fig. 3.** Summary of fossil coral uranium isotope results. (a)  $\{\text{<sup>234</sup>U}/\text{<sup>238</sup>U}\}$  in fossil corals vs. sample age. Colors correspond to fossil coral [U]. Circled samples are fossils flagged based on  $\{\text{<sup>234</sup>U}/\text{<sup>238</sup>U}\}$  that are offset beyond analytical uncertainty from secular equilibrium. Error bars correspond to  $2\sigma$  s.d. for Nod-A-1. (b)  $\delta^{238}/\text{<sup>235</sup>U}$  in fossil corals vs. sample age. Colors as in (a). Circled samples correspond to those flagged based on  $\delta^{238}/\text{<sup>235</sup>U}$  ratios that deviate from the modern coral average beyond uncertainty. Error bar for corals correspond to the long-term reproducibility of the standard, Nod-A-1 ( $\pm 0.1\text{\textperthousand}$   $2\sigma$  s.d.). Ferromanganese crust records from Goto et al. (2014) and Wang et al. (2016a) are also plotted and are offset by  $+0.26\text{\textperthousand}$  for direct comparison with modern coral and modern seawater. Long term external reproducibility of standards for Wang et al. (2016a) data was  $\pm 0.09\text{\textperthousand}$  and  $\pm 0.11\text{\textperthousand}$  for data from Goto et al. (2014).

In addition to He/U and  $\{\delta^{234}\text{U}/\delta^{238}\text{U}\}$ , we use coral  $\delta^{238}/\delta^{235}\text{U}$  compositions as a constraint on fossil coral preservation. Existing records from Fe-Mn crusts suggest seawater  $\delta^{238}/\delta^{235}\text{U}$  has likely remained within  $\pm 0.09\text{\textperthousand}$  of the modern seawater composition over the last  $\sim 80$  million years (Goto et al., 2014; Wang et al., 2016a). Assuming that  $\delta^{238}/\delta^{235}\text{U}$  fractionation between seawater and coral has not changed with time, there are six fossil coral samples we measure that deviate by more than  $\pm 0.09\text{\textperthousand}$  from the modern coral average of  $-0.37\text{\textperthousand}$  toward heavier  $\delta^{238}/\delta^{235}\text{U}$ . Five of these fossil samples also deviate from the modern coral average beyond analytical uncertainty based on the reproducibility of the Fe-Mn standard Nod-A-1 (Fig. 3b, Table 3). Recent work shows that diagenesis of carbonate sediments in the presence of reducing pore fluids can cause an increase in carbonate [U] and a  $\sim 0.25\text{\textperthousand}$  shift in carbonate  $\delta^{238}/\delta^{235}\text{U}$  toward heavier values (Romaniello et al., 2013; Chen et al., 2018b; Tissot et al., 2018). Chen et al. (2018b) suggest that recrystallization of biogenic aragonite in seawater or marine pore fluids can also result in a shift toward heavier  $\delta^{238}/\delta^{235}\text{U}$ . While there is no obvious evidence of neomorphism or diagenetic cements for these five samples based on previous diagenetic screening (Gothmann et al., 2015), the magnitude of the offset in  $\delta^{238}/\delta^{235}\text{U}$  for these samples as compared with modern fossil corals is general consistent with the diagenetic offsets observed in modern carbonate sediments (Romaniello et al., 2013; Chen et al., 2018b; Tissot et al., 2018). We note, however, that samples with heavy  $\delta^{238}/\delta^{235}\text{U}$  do not have anomalously high U/Ca as compared with samples of similar age (see supplementary Fig. S4). This observation suggests that if our heavy coral  $\delta^{238}/\delta^{235}\text{U}$  are not primary, then their compositions may reflect the addition of a small amount of secondary U that is extremely enriched in  $^{238}\text{U}$ . Their compositions could also be explained by replacement of primary coral uranium with a fluid of different  $\delta^{238}/\delta^{235}\text{U}$  and similar [U]. We flag these samples in our reconstruction of seawater U/Ca to acknowledge the possibility that these samples may have a diagenetic uranium component (Table 3). Excluding these samples, fossil corals measured in this study yield an average  $\delta^{238}/\delta^{235}\text{U}$  of  $-0.34 \pm 0.11\text{\textperthousand}$  ( $2\sigma$  s.d.;  $n = 14$ ) – close to the modern coral average of  $-0.37\text{\textperthousand}$  (Fig. 3b, Table S2). Fig. 3b also shows that fossil corals exhibit a  $\sim 0.05\text{\textperthousand}$  change in  $\delta^{238}/\delta^{235}\text{U}$  between modern samples and Eocene samples, with Eocene samples being higher, although this change is not statistically significant (Welch's t-test,  $p > 0.05$ ).

Elevated  $\delta^{238}/\delta^{235}\text{U}$  values in Eocene fossil corals could reflect an increase in  $^{238}\text{U}/^{235}\text{U}$  fractionation between corals and contemporaneous seawater. Reconstructions of seawater pH suggest that it has increased by 0.3–0.4 pH units between the Early Cenozoic and present (Hönisch et al., 2012). In addition, inorganic aragonite precipitation experiments and uranium speciation modeling studies suggest that  $^{238}/^{235}\text{U}$  fractionation depends on pH as well as seawater Ca and Mg concentrations, with a  $<0.06\text{\textperthousand}$  decrease in carbonate  $\delta^{238}/\delta^{235}\text{U}$  predicted between the early Cenozoic and today (Chen et al., 2016; 2017). The  $0.05\text{\textperthousand}$  change observed between modern and Eocene samples in this study is generally com-

patible with the decrease in U isotope fractionation predicted by Chen et al. (2017).

### 3.3. Fossil coral U/Ca record

Fossil coral U/Ca data are presented in Table 2 and Fig. 4a, b. U/Ca ratios are low for early Cenozoic samples, and increase by a factor of 4–5 between the Eocene and the present. Trends are similar for flagged and included samples, although flagged samples are more scattered. Our coral U/Ca record must reflect either (1) large changes in U uptake dynamics in coral aragonite through time, or (2) changes in the U/Ca ratio of seawater. We evaluate these two possibilities below.

Culture experiments and surveys of natural coral samples indicate that the U/Ca ratio of the aragonitic coral skeleton is anti-correlated with the pH and/or  $[\text{CO}_3^{2-}]$  of the growth medium (Armid et al., 2008; Anagnostou et al., 2011; Inoue et al., 2011; Raddatz et al., 2014). A similar dependence has been demonstrated for inorganic aragonite (Meece and Benninger, 1993; DeCarlo et al., 2015) and many other biogenic carbonates (e.g., Russell et al., 1994; Keul et al., 2013). The inorganic growth experiments of DeCarlo et al. (2015) suggest that the relationship arises due to a predominant dependence on  $[\text{CO}_3^{2-}]$  and not pH; the apparent pH dependences observed in other studies arise from the co-variation of  $[\text{CO}_3^{2-}]$  and pH at constant DIC.

The sensitivity of coral U/Ca to  $[\text{CO}_3^{2-}]$  (or pH), differs between surface (usually zooxanthellate/symbiotic) and deep-sea corals (usually azooxanthellate/asymbiotic). Deep-sea corals exhibit a range in the U/Ca ratio of  $\pm 50\%$  among natural samples collected from waters with pH ranging between 7.5 and 8.3, and most of the variance is linked to  $[\text{CO}_3^{2-}]$  (or pH) (Anagnostou et al., 2011; Raddatz et al., 2014). In contrast, culture experiments with symbiotic (zooxanthellate) surface corals suggest a much more moderate dependence on seawater carbonate chemistry, with bulk coral U/Ca ranging by  $\sim \pm 8\%$  over a pH range of 7.3 to 8.0, and a slope of  $-0.21 \mu\text{mol/mol U/Ca pH}^{-1}$  (Inoue et al., 2011). The sensitivity of inorganic aragonite U/Ca to seawater  $[\text{CO}_3^{2-}]$  is also about an order of magnitude less than the sensitivity observed for deep-sea corals (DeCarlo et al., 2015). We assume that all corals in our sample set would respond to changes in seawater pH with the sensitivity of shallow water corals ( $-0.21 \mu\text{mol/mol pH}^{-1}$ ; Inoue et al., 2011) – similar to inorganic aragonite. This may not be a good assumption as our fossil coral samples are a mixture of symbiotic and asymbiotic species (see Table 2). However, measured U/Ca ratios are similar for both asymbiotic and symbiotic fossil coral samples, suggesting that any systematic difference in sensitivity to seawater pH is small (Fig. 4).

Many independent studies have concluded that seawater pH and  $[\text{CO}_3^{2-}]$  was 0.3–0.4 units and a factor of  $\sim 3$  lower (respectively) than present during the early Cenozoic (Tyrrell and Zeebe, 2004; Ridgwell and Zeebe, 2005; Hönisch et al., 2012; Zeebe, 2012; Hain et al., 2015). As detailed in Hain et al. (2015), these changes are compatible with current views that  $\text{pCO}_2$  was high in the early Cenozoic, seawater DIC similar to present, and seawater [Ca]

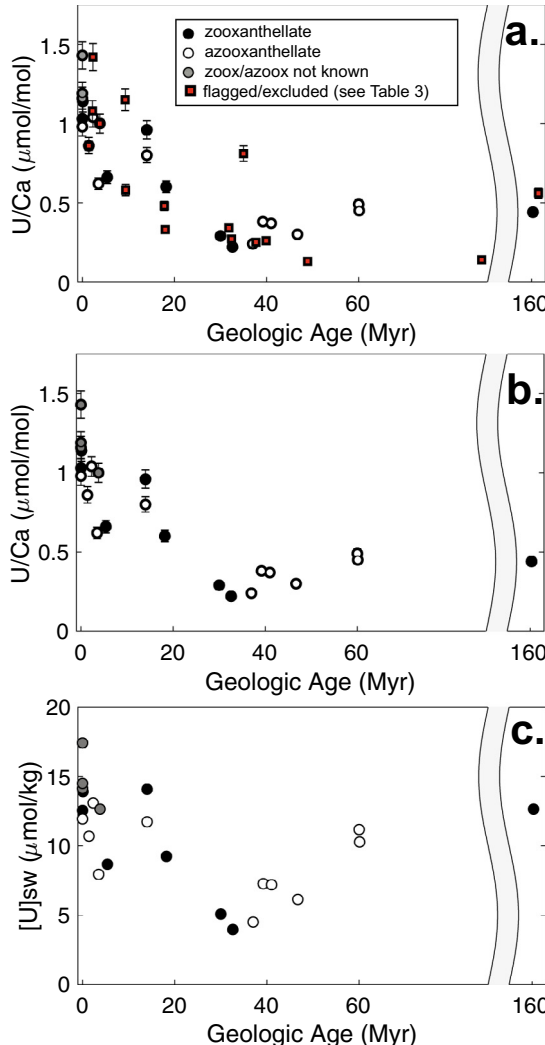


Fig. 4. (a) Measured U/Ca of fossil corals vs. geologic age. Coral U/Ca increases by a factor of 4–5 since ~30 Ma. Error bars correspond to  $2\sigma$  s.d. (b) Same as in (a), but removing samples with anomalous characteristics (see text). (c) Estimates of seawater [U] calculated by assuming a constant U/Ca distribution coefficient for corals of 0.87 (Broecker, 1971; Meece and Benninger, 1993; Min et al., 1995; Shen and Dunbar, 1995) as well as that seawater [Ca] decreased linearly from 26 mmol/kg to 10.6 mmol/kg between 100 Ma and today (Horita et al., 2002; Lowenstein et al., 2003; Sarmiento and Gruber, 2006; Timofeeff et al., 2006). We choose 100 Ma as the start of the seawater [Ca] decline because there are no estimates for seawater [Ca] from fluid inclusions between 100 Ma and ~35 Ma (Zimmerman, 2000; Horita et al., 2002; Lowenstein et al., 2003; Timofeeff et al., 2006; Brennan et al., 2013). It is also assumed that [Ca] = 23 mM at 160 million years ago for our Jurassic samples, based on fluid inclusion estimates from Timofeeff et al. (2006). We note that this reconstruction of seawater [U] depends on the quality of reconstructions of seawater [Ca]. Black circles correspond to zooxanthellate samples, white circles correspond to azooxanthellate samples, grey circles correspond to samples for which symbiont status is unknown (as given in Table 2). Red squares correspond to samples that have been excluded or flagged due to the possibility of alteration of original U geochemistry as indicated by uranium isotopes and He/U ages (see Table 3). (For interpretation of the references to colour in this figure legend, the reader is referred to the web version of this article.)

was elevated (Horita et al., 2002; Lowenstein et al., 2003; Brennan et al., 2013). Applying the  $-0.21 \mu\text{mol/mol pH}^{-1}$  dependence from modern shallow-water zooxanthellate corals (Inoue et al., 2011) and assuming no change in seawater U/Ca we estimate that coral U/Ca would have been  $\sim 0.08 \mu\text{mol/mol}$  higher during the early Cenozoic than today. This small change would be difficult to resolve given the natural range of variability observed for modern surface corals – (0.8–2  $\mu\text{mol/mol}$ ) (Swart and Hubbard, 1982; Min et al., 1995). Instead, we observe that coral U/Ca ratios are much *lower* in samples from the early Cenozoic (Fig. 4) – a change that is the opposite sign to that predicted from reconstructions of seawater pH and  $[\text{CO}_3^{2-}]$ . As a result, the coral U/Ca data do not appear to be related to changes in coral U uptake associated with secular change in seawater pH or  $[\text{CO}_3^{2-}]$  over the Cenozoic. Instead, we favor the alternative explanation that the data reflect an increase in the U/Ca ratio of seawater.

Determining the magnitude of the increase in seawater U/Ca from our fossil coral record depends on whether coral U/Ca is predominantly dependent on seawater [U] (Swart and Hubbard, 1982; Shen and Dunbar, 1995), or on the seawater U/Ca ratio (Broecker, 1971; Meece and Benninger, 1993; Gabitov et al., 2008). In the first case, our record would suggest a factor of 4–5 increase in seawater uranium concentrations between the Paleocene and today. In the second case, changes in seawater [Ca] or changes in seawater [U] could drive the coral chemistry we observe. Seawater [Ca] has decreased by a factor of  $\sim 2.5$  since  $\sim 100$  Ma (Lowenstein et al., 2001; 2003; Dickson, 2002; 2004; Horita et al., 2002; Timofeeff et al., 2006; Coggon et al., 2010; Rausch et al., 2013; Gothmann et al., 2015), suggesting that roughly half of the increase in coral U/Ca could be due to changes in seawater Ca. The remainder of the increase in U/Ca then only requires that [U] has risen by a factor of 1.5–2.

Fig. 4c plots our preferred reconstruction of seawater [U] from fossil corals, calculated assuming that coral U/Ca depends on seawater U/Ca with a partition coefficient ( $K_{\text{U/Ca,sw-coral}}^D$ ) of 0.87 based on the average of modern corals measured in this study. To calculate seawater [U], we assume that seawater [Ca] decreased linearly from 26 mmol/kg to 10.6 mmol/kg between 100 Ma and today, as broadly suggested by fluid inclusions trapped in halite (see Fig. 5b; Horita et al., 2002; Lowenstein et al., 2003; Sarmiento and Gruber, 2006; Timofeeff et al., 2006). We choose 100 Ma as the start of the seawater [Ca] decline because there are no estimates for seawater [Ca] from fluid inclusions between 100 Ma and ~35 Ma (Zimmerman, 2000; Horita et al., 2002; Lowenstein et al., 2003; Timofeeff et al., 2006; Brennan et al., 2013). From only two Paleocene samples, our coral data suggest a  $\sim 50\%$  decrease in seawater [U] from the Paleocene to the middle Oligocene. Subsequently, U rises by a factor of  $\sim 2$  between  $\sim 40$  Ma and today.

### 3.4. Secular variations in seawater [U]

The abundance of U in seawater reflects a balance between uranium sources and sinks:

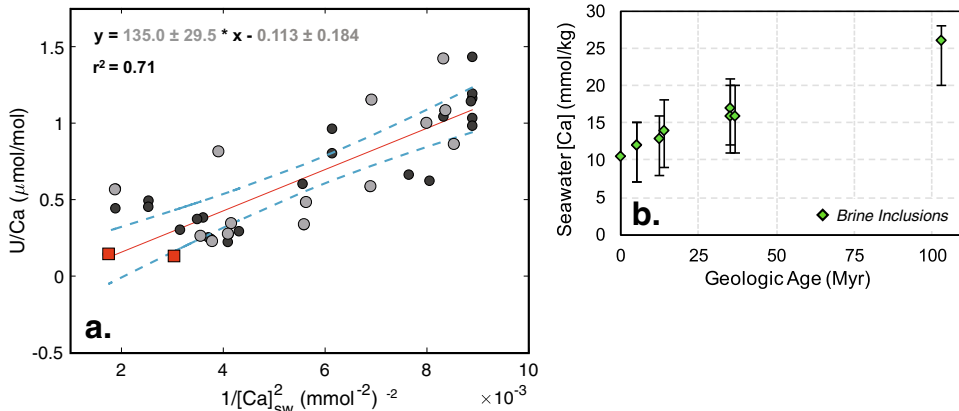


Fig. 5. (a) Comparison plot showing linear relationship between  $U/Ca_{\text{coral}}$  and  $1/[Ca]_{\text{sw}}^2$  as suggested by Broecker (1971). Seawater [Ca] is estimated assuming a linear decrease in seawater [Ca] from 26 mmol/kg to 10.6 mmol/kg between 100 Ma and today as supported by brine inclusion data displayed in (b) (Horita et al., 2002; Lowenstein et al., 2003; Sarmiento and Gruber, 2006; Timofeeff et al., 2006). We also assume that seawater [Ca] = 23 mmol/kg at 160 Ma for our Jurassic fossil coral samples. Samples flagged based on He/U or U isotope data are shown in grey, samples excluded based on the presence of calcite are shown in red. The red line represents the linear fit to the data and the blue dashed lines are the 95% confidence intervals. (For interpretation of the references to colour in this figure legend, the reader is referred to the web version of this article.)

$$dU_{\text{sw}}/dt = F_{\text{inputs}} - F_{\text{outputs}}, \quad (3)$$

$$dU_{\text{sw}}/dt = F_{\text{River}} - (F_{\text{Low-T Hydrothermal}} + F_{\text{Anoxic}} + F_{\text{Suboxic}} + F_{\text{Carbonate}} + F_{\text{Coastal and Fe-Mn}}), \quad (4)$$

where the term  $U_{\text{sw}}$  represents the abundance of uranium in seawater (mol), and  $F_x$  terms represent the U mass fluxes associated with various sources and sinks (mol/yr). The only significant source of U to seawater is  $F_{\text{river}}$ , the flux of U from chemical weathering on the continents. U sinks include  $F_{\text{Low-T Hydrothermal}}$ , the removal of seawater U in low-temperature hydrothermal systems, and  $F_{\text{Anoxic}}$  and  $F_{\text{Suboxic}}$  the U sinks in anoxic and suboxic sediments, respectively. The term  $F_{\text{Carbonate}}$  corresponds to the U flux buried in carbonate sediments, and  $F_{\text{Coastal and Fe-Mn}}$  corresponds to the U flux in coastal wetland sediments and in Fe-Mn crusts (Dunk et al., 2002; Tissot and Dauphas, 2015). There exists disagreement as to the magnitude of the carbonate uranium sink, with estimates ranging from  $\sim 5$  to  $\sim 25$  % of the total seawater uranium sink (Barnes and Cochran, 1990; Klinkhammer and Palmer, 1991; Morford and Emerson, 1999; Dunk et al., 2002) (see also Table 1).

### 3.4.1. A relationship between seawater [U] and seawater $[CO_3^{2-}]$

In the following sections, we discuss the possible controls on Cenozoic seawater [U] in further detail. First, we consider a hypothesis proposed by Broecker (1971) and Broecker (2013), which suggests that the magnitudes of U removal in the major oceanic sinks (carbonate sediments, anoxic/suboxic sediments, Fe-Mn crusts, alteration of basalt) are all dependent on seawater  $[CO_3^{2-}]$ . Broecker's hypothesis is grounded in studies of the [U] of highly alkaline Mono Lake, which has both  $[CO_3^{2-}]$  and [U]  $\sim 100$  times greater than seawater (Thurber, 1965; Anderson et al., 1982; Simpson, 1982). Similarly high U concentra-

tions have been observed in alkaline surface waters of Eastern and Western Mongolia (Linhoff et al., 2011; Shvartsev et al., 2012). According to Broecker (1971) and Broecker (2013), observations of the correlation between [U] and  $[CO_3^{2-}]$  in alkaline lakes suggest that an increase in seawater  $[CO_3^{2-}]$  could be accompanied by a proportional increase in seawater [U]. Importantly, because of the long residence time of U in seawater ( $\sim 400,000$  yrs; Chen et al., 1986), this control is only relevant over million-year timescales.

Broecker (1971) and (2013) further suggested that if seawater [U] is indeed controlled by seawater  $[CO_3^{2-}]$ , then coral U/Ca should scale with past seawater  $[CO_3^{2-}]$  and/or seawater [Ca]. As shown in the equations below, this relationship assumes that the U/Ca ratio of corals records the U/Ca ratio of seawater, that seawater [U] is proportional to seawater  $[CO_3^{2-}]$ , and that the saturation state of seawater has not varied greatly over the Cenozoic (Tyrrell and Zeebe, 2004):

$$U/Ca_{\text{corals}} \approx U/Ca_{\text{sw}} \text{ and } [U]_{\text{sw}} \propto [CO_3^{2-}]_{\text{sw}}, \quad (5)$$

$$U/Ca_{\text{corals}} \propto [CO_3^{2-}]_{\text{sw}}/[Ca]_{\text{sw}}, \quad (6)$$

$$[Ca]_{\text{sw}} \times [CO_3^{2-}]_{\text{sw}} = \text{constant}, \quad (7)$$

$$U/Ca_{\text{corals}} \propto 1/[Ca]_{\text{sw}}^2, \quad (8)$$

Eq. (8) suggests that fossil coral U/Ca should be linearly proportional to  $1/[Ca]_{\text{sw}}^2$ . We plot this relationship in Fig. 5 for our samples, where  $[Ca]_{\text{seawater}}$  is calculated assuming a linear decrease in seawater [Ca] from 26 mmol/kg to 10.6 mmol/kg between 100 Ma and today, as in Fig. 4c (Horita et al., 2002; Lowenstein et al., 2003; Timofeeff et al., 2006; Sarmiento and Gruber, 2006). The observed linear relationship displayed in Fig. 5 between  $U/Ca_{\text{coral}}$  and  $1/[Ca]_{\text{sw}}^2$  is generally compatible with the Broecker hypothesis.

There is good reason to expect seawater [U] to depend on  $[CO_3^{2-}]$ . Uranium's propensity to complex with carbon-

ate in natural waters, and with cations such as Ca, increases its solubility (Langmuir, 1978; Bernhard et al., 2001; Dong and Brooks, 2006; Endrizzi and Rao, 2014) and virtually all dissolved U in seawater exists as a  $\text{CO}_3^{2-}$  complex (Langmuir, 1978; Djogic et al., 1986; Reeder et al., 2000; Endrizzi and Rao, 2014). The dominant forms of uranium in seawater at  $\text{pH} > 6$  are  $\text{Ca}_2\text{UO}_2(\text{CO}_3)_3(\text{aq})$  (~55% of total uranium),  $\text{MgUO}_2(\text{CO}_3)_3^{2-}$  (~20% of total uranium),  $\text{CaUO}_2(\text{CO}_3)_3^{2-}$  (~20% of total uranium), and  $\text{UO}_2(\text{CO}_3)_3^{4-}$  (~5% of total uranium) (Endrizzi and Rao, 2014).

In addition to the relationships between  $[\text{U}]$  and  $[\text{CO}_3^{2-}]$  observed in alkaline lakes, recent experimental evidence suggests that the magnitude of U removal in many major sinks (e.g., carbonate sediments, reducing sediments, and Fe-Mn crusts) could be limited by higher  $[\text{CO}_3^{2-}]$ . As described earlier, the U partition coefficient for both biogenic and inorganic calcium carbonate is observed to decrease with increasing carbonate ion concentrations (Russell et al., 1994; Armid et al., 2008; Anagnostou et al., 2011; Inoue et al., 2011; Raddatz et al., 2014; DeCarlo et al., 2015). Furthermore, experimental studies indicate that the reduction of U(VI) to U(IV) appears to be inhibited by higher  $[\text{CO}_3^{2-}]$  for both abiotic and biologically-mediated reduction (Belli et al., 2015; Hua et al., 2006). These uranium reduction experiments show that the highest reaction rates for U reduction are associated with solutions dominated by 'free' uranium and uranium-hydroxide species, while lower reduction rates are associated with solutions dominated by  $\text{UO}_2\text{-CO}_3$  species. Thus, the presence of  $[\text{CO}_3^{2-}]$  in solution limits uranium reduction because the fractional abundance of uranium-hydroxyl species is lower at high  $[\text{CO}_3^{2-}]$  (Hua et al., 2006; Belli et al., 2015). Finally, Wazne et al. (2003) found that the amount of U(VI) adsorbed on ferrihydrite was a strong function of the concentration of carbonate ion in solution, indicating that uranium removal from seawater in oxic sinks should also decrease with increasing  $[\text{CO}_3^{2-}]$ .

#### 3.4.2. Changes in the uranium river flux due to Himalayan uplift

Changes in the uranium river flux – the main input source of U to seawater (Eq. (3)) – also likely contributed to variations in seawater  $[\text{U}]$  over the Cenozoic. Rivers carry uranium derived predominantly from the weathering of carbonates and uraniferous black shales, (Palmer and Edmond, 1993), and the Ganges and Brahmaputra rivers draining the Himalayas are particularly enriched in uranium relative to other large rivers. However, seasonally averaged studies suggest that these rivers only make up ~10% of the modern global uranium river flux (Sarin et al., 1990; Palmer and Edmond, 1993; Chabaux et al., 2001; Dunk et al., 2002; Andersen et al., 2016). Therefore, although Himalayan uplift may have contributed to the rise in seawater  $[\text{U}]$  between the Early Cenozoic and present, it is unlikely that it can account for the majority of the increase we observe.

#### 3.4.3. Changes in low-temperature hydrothermal alteration

Changes in hydrothermal alteration through time may also be able to drive the changes in seawater  $[\text{U}]$  we infer

from our coral record. Uranium is quantitatively stripped from hydrothermal fluids during high-temperature hydrothermal alteration at the ridge axis (Michard et al., 1983; Michard and Albarede, 1985). However, due to the relatively small water flux associated with high-temperature hydrothermal alteration ( $2.6 \pm 0.5 \times 10^{12} \text{ m}^3/\text{yr}$  as compared with the river flux:  $4-5 \times 10^{13} \text{ m}^3/\text{yr}$ ), this sink of uranium is minor (Elderfield and Schultz, 1996). In contrast, low-temperature hydrothermal alteration, for which the water flux is estimated to range from  $4.8 - 21.0 \times 10^{12} \text{ m}^3/\text{yr}$ , constitutes a major sink of uranium from seawater (Table 1; Fig. 6; Barnes and Cochran, 1990; Klinkhammer and Palmer, 1991; Dunk et al., 2002; James et al., 2003; Wheat et al., 2003; Mills and Dunk, 2010). The alteration products in which U is incorporated are likely palagonites, smectites, and Fe-oxides (MacDougall, 1977; Mills and Dunk, 2010; Noordmann et al., 2015).

Recent studies have highlighted the potential importance of variations in low-temperature ridge-flank hydrothermal alteration for the seawater budgets of elements like Mg, Sr, Ca, and Li. For example, it has been suggested that changes in ocean bottom water temperatures over the Cenozoic due to global cooling could explain observed variations in Cenozoic seawater Mg/Ca and  $\delta^{26}\text{Mg}$  (Higgins and Schrag, 2015). Indeed, the observation

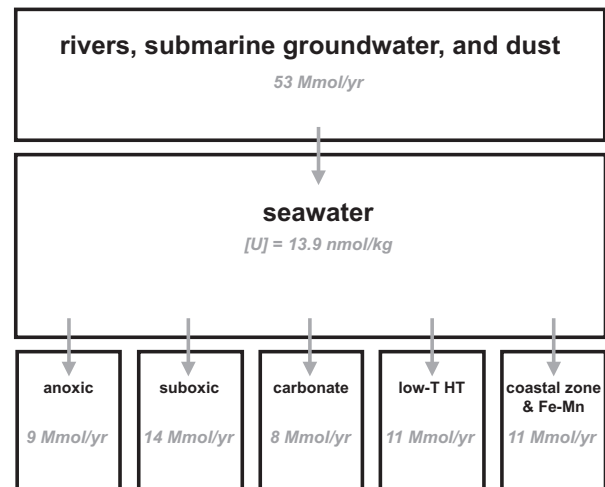


Fig. 6. Schematic of the modern seawater uranium mass balance used for the steady-state calculations in Sections 3.4.3 and 3.4.4, adapted from Barnes and Cochran (1990), Klinkhammer and Palmer (1991), and Dunk et al. (2002) in accordance with updated constraints on the low-T hydrothermal and anoxic sinks (Wheat et al., 2003; Mills and Dunk, 2010; Montoya-Pino et al., 2010; Brennecke et al., 2011; Noordmann et al., 2015).  $\delta^{238}\text{U}$  compositions relative to CRM112a and isotope effects associated with depicted sink terms ( $\Delta^{238}\text{sink} = \delta^{238}\text{Usink} - \delta^{238}\text{Useawater}$ ) are as follows:  $\delta^{238}\text{U}_{\text{river}} = -0.24\text{\textperthousand}$ ,  $\Delta^{238}\text{anoxic} = +0.60\text{\textperthousand}$ ,  $\Delta^{238}\text{suboxic} = +0.10\text{\textperthousand}$ ,  $\Delta^{238}\text{low-T hydrothermal} = +0.23\text{\textperthousand}$ ,  $\Delta^{238}\text{Coastal Retention and Fe-Mn} = -0.24\text{\textperthousand}$ ,  $\Delta^{238}\text{Carb} = 0.20\text{\textperthousand}$  (Weyer et al., 2008; Montoya-Pino et al., 2010; Noordmann et al., 2015; Tissot and Dauphas, 2015). Solving the budget depicted in this figure yields a value for  $\delta^{238}\text{U}_{\text{ModernSW}} = -0.396\text{\textperthousand}$ , consistent with values reported in Tissot and Dauphas (2015).

that  $[Mg]$  and  $[U]$  are correlated in low-T hydrothermal fluids (Wheat et al., 2003; Noordmann et al., 2015) suggests that similar kinetics may govern the removal of both elements.

A steady-state calculation allows us to investigate the magnitude of change in the low-temperature hydrothermal alteration sink required to drive a change in seawater  $[U]$  between 40 Ma and today (Fig. 4c). We assume modern seawater uranium fluxes given in Fig. 6. The budget described in Fig. 6 generally follows from Dunk et al. (2002), but has been updated in accordance with more recent constraints on the low-T hydrothermal and anoxic sinks (Wheat et al., 2003; Mills and Dunk, 2010; Montoya-Pino et al., 2010; Brennecke et al., 2011; Noordmann et al., 2015). The hydrothermal flux is  $\sim 21\%$  of total U removal – well within the range of 15–70% estimated by Barnes and Cochran (1990), Morford and Emerson (1999), James et al. (2003), Wheat et al. (2003), and Mills and Dunk (2010). We also assume that the riverine U input remains constant through time, and that all seawater sinks are first-order with respect to the seawater  $[U]$ :

$$F_{\text{sink}} = k_{\text{sink}} \times [U]_{\text{seawater}}, \quad (9)$$

where  $F_{\text{sink}}$  is the flux of U into the seawater sink (e.g.,  $F_{\text{Low-T Hydrothermal}}$ ,  $F_{\text{Coastal Retention}}$ ,  $F_{\text{Anoxic}}$ , and  $F_{\text{Suboxic}}$  in Eq. (4)),  $k_{\text{sink}}$  is the removal rate constant associated with each sink. The steady state uranium budget can be written as below, following from Eqs. (3), (4), and (9) and assuming constant seawater volume:

$$\begin{aligned} F_{\text{Low-T Hydrothermal}} \\ = F_{\text{River}} - (k_{\text{anoxic}} \times [U]_{\text{seawater}} + k_{\text{suboxic}} \times [U]_{\text{seawater}} \\ + k_{\text{carbonate}} \times [U]_{\text{seawater}} + k_{\text{Coastal and Fe - Mn}} \times [U]_{\text{seawater}}), \end{aligned} \quad (10)$$

The values used for our rate constants ( $k_{\text{sink}}$ ) are based on estimates of modern fluxes shown in Fig. 6. These  $k_{\text{sink}}$  terms are assumed to remain constant with time for these calculations. Following the equation above, a doubling of seawater  $[U]$  between 40 Ma and today, requires a  $\sim 65\%$  decrease in the low-temperature hydrothermal uranium sink, assuming rate constants for the other seawater uranium sinks remain unchanged.

The magnitude of change in the hydrothermal flux we calculate is broadly consistent with the factor of 2 change in low temperature hydrothermal Mg flux modeled by Higgins and Schrag (2015) between the early Cenozoic and today to explain observed variations in seawater Mg/Ca and  $\delta^{26}\text{Mg}$ . These calculations allow for a possibility that changes in the hydrothermal flux play a major role in driving the inferred variations in seawater  $[U]$  although our predictions here and in Section 3.4.4 and Section 3.4.5 below will be sensitive to the rate constants ( $k$  values) chosen for our calculations. Section 3.4.5 also discusses additional constraints from U isotopes. We also note that it is unclear whether temperature or redox is the main factor in determining the uptake of U from seawater during low temperature hydrothermal alteration (Dunk et al., 2002; James et al., 2003; Mills and Dunk, 2010). Recently, based on  $\delta^{238/235}\text{U}$  isotope analyses of basalt altered at low temperatures and

hydrothermal fluids, Andersen et al. (2015) and Noordmann et al. (2015) suggested that some hydrothermal U removal likely occurs via oxic weathering (where temperature may determine reaction kinetics) and some occurs through reduction of U(VI) to U(IV) by reducing hydrothermal fluids. Additional studies of the controls on the hydrothermal U sink may better help determine the importance of this flux in changing seawater  $[U]$  over the Cenozoic.

### 3.4.4. A dependence of seawater $[U]$ on ocean $O_2$

Finally, we explore the possibility that a decrease in the uranium flux to suboxic and anoxic sediments can explain our record. Like low-temperature hydrothermal alteration, suboxic and anoxic sediments are important sinks for seawater U (Fig. 6 and Table 1). Here we define suboxic sediments as having no oxygen or  $H_2S$  (e.g., the Peru margin), while anoxic sediments are defined as having  $H_2S$  present and no oxygen (e.g., the Black Sea) (Berner, 1981; Crusius et al., 1996). The U concentration of suboxic and anoxic sediments has been linked to a variety of factors including: (1) the magnitude of the organic matter flux and organic carbon burial (McManus et al., 2005; McManus et al., 2006; Morford et al., 2009), (2) uranium adsorbed to organic material in the surface ocean that escapes remineralization at depth (Zheng et al., 2002), and (3) microbially-mediated reduction of U(VI) to U(IV) with subsequent precipitation of solid uranium phases (Lovley et al., 1991). To first order, however, the dominant control on U removal in suboxic and anoxic sediments is likely the oxygen concentration of ocean bottom waters (Anderson, 1987; Barnes and Cochran, 1990; Morford and Emerson, 1999; Weyer et al., 2008).

Changes in the fluxes of U to anoxic and suboxic sediments, resulting (for example) from changes in ocean oxygenation or productivity, may drive changes in seawater  $[U]$ . Analogous to Eq. (10) above, we can solve for the magnitude of change in the suboxic and anoxic fluxes required to drive a factor of 2 increase in seawater  $[U]$  between 40 Ma and today. For simplicity, we link the suboxic and anoxic fluxes (i.e., increasing the suboxic sink by 10%, also increases the anoxic sink by 10%):

$$\begin{aligned} F_{\text{anox}} + F_{\text{subox}} \\ = F_{\text{River}} - (k_{\text{Low-T Hydrothermal}} \times [U]_{\text{seawater}} \\ + k_{\text{carbonate}} \times [U]_{\text{seawater}} + k_{\text{Coastal and Fe - Mn}} \times [U]_{\text{seawater}}) \end{aligned} \quad (11)$$

Assuming that the rate constants associated with other uranium sinks stay constant, this calculation suggests that the suboxic and anoxic fluxes of U must have decreased by  $\sim 40\%$  between 40 Ma and today in order to account for the changes in seawater  $[U]$  we observe.

### 3.4.5. Constraints from seawater $\delta^{238/235}\text{U}$

Any explanation for the rise in U/Ca ratios over the Cenozoic must also be consistent with records of seawater  $\delta^{238/235}\text{U}$  over this time period. Two existing records of Cenozoic seawater  $\delta^{238/235}\text{U}$  show that the isotopic composition of seawater has remained constant to within error of the method ( $\sim \pm 0.09\text{\textperthousand}$ ), consistent with the coral data pre-

sented here (Goto et al., 2014; Wang et al., 2016a). To explore whether a decline in the suboxic and anoxic sinks or the low temperature hydrothermal flux is consistent with the existing records of seawater  $\delta^{238/235}\text{U}$ , Eqs. (3) and (4) can be amended to include U isotopes and solved at steady-state ( $d[\delta^{238/235}\text{U}_{\text{sw}}]/dt = 0$ ) to produce the steady state uranium isotope mass balance for seawater:

$$\begin{aligned} (\delta^{238/235}\text{U}_{\text{River}}) = & f_{\text{Low-T Hydrothermal}} \times (\delta^{238/235}\text{U}_{\text{sw}} \\ & + \Delta_{\text{Low-T Hydrothermal}}^{238}) + f_{\text{anoxic}} \\ & \times (\delta^{238/235}\text{U}_{\text{sw}} + \Delta_{\text{anoxic}}^{238}) + f_{\text{suboxic}} \\ & \times (\delta^{238/235}\text{U}_{\text{sw}} + \Delta_{\text{suboxic}}^{238}) + f_{\text{carbonate}} \\ & \times (\delta^{238/235}\text{U}_{\text{sw}} + \Delta_{\text{carbonate}}^{238}) \\ & + f_{\text{Coastal and Fe-Mn}} \times (\delta^{238/235}\text{U}_{\text{sw}} \\ & + \Delta_{\text{Coastal and Fe-Mn}}^{238}), \end{aligned} \quad (12)$$

where  $\Delta_{\text{sink}}^{238} = \delta^{238}\text{U}_{\text{sink}} - \delta^{238}\text{U}_{\text{seawater}}$ , and  $f_{\text{sink}}$  is the fraction of the total uranium output associated with each sink term. It is important to note that this steady state model is applicable only on timescales  $>10^6$  yrs. Although there exist minor disagreements in the isotopic compositions associated with uranium sink and source terms for recently published U isotope budgets, there is clear consensus that (1) the U isotope system can be used to track the extent of anoxic and suboxic conditions and (2) an expansion of anoxia should result in both a decrease of seawater [U] and  $\delta^{238}\text{U}$  (e.g. Brennecke et al., 2011; Tissot and Dauphas, 2015; Andersen et al., 2016; Clarkson et al., 2018). Here, we choose the U isotope budget given in Tissot and Dauphas (2015) (see Fig. 6 caption for values), which would predict a modern seawater  $\delta^{238/235}\text{U}$  of  $-0.40\text{\textperthousand}$  for our modern budget, similar to measured modern seawater compositions (Noordmann et al., 2015; Tissot and Dauphas, 2015). Using Eq. (13) we predict a  $\sim 0.04\text{\textperthousand}$  increase in  $\delta^{238/235}\text{U}_{\text{sw}}$  between 40 Ma and today assuming the low-temperature hydrothermal flux was 65% higher at 40 Ma. A  $\sim 0.07\text{\textperthousand}$  increase in  $\delta^{238/235}\text{U}_{\text{sw}}$  between 40 Ma and today is predicted assuming that the suboxic and anoxic uranium fluxes were  $\sim 40\%$  higher at 40 Ma. However, we note that our approach of assuming that suboxic/anoxic sinks expanded together is conservative, given evidence that anoxic areas, which are characterized by largest effective fractionation during U burial, will expand at the expense of suboxic areas during a shift to a more reducing marine redox landscape (Wang et al., 2016b). We also note that our prediction is sensitive to the choice of the mean fractionation associated with the anoxic uranium sink, and that recent studies have suggested values ranging from  $+0.4$  to  $0.85\text{\textperthousand}$  (Weyer et al., 2008; Basu et al., 2014; Noordmann et al., 2015; Tissot and Dauphas, 2015; Stylo et al., 2015; Andersen et al., 2016).

Considering the existing uncertainties associated with the Fe-Mn crust records and the possibility of open-system exchange with seawater ( $\pm 0.09\text{\textperthousand}$ ), it is unclear whether the low-T hydrothermal scenario described in Section 3.4.3 or the changing suboxic/anoxic sink scenario (Section 3.4.4) can be ruled out based on the predicted

$\sim 0.04\text{\textperthousand}$  and  $\sim 0.07\text{\textperthousand}$  increase, respectively (see Fig. 3b; Goto et al., 2014; Wang et al., 2016a). Additional high-fidelity and high-precision records of Cenozoic seawater  $\delta^{238/235}\text{U}_{\text{sw}}$  may provide additional constraints on the relative importance of mechanisms considered here.

#### 4. CONCLUSIONS

Uranium concentrations in seawater are tightly linked with the cycling of carbon and oxygen – two globally important elements. In this paper, we present a new reconstruction of seawater U/Ca from fossil corals that span the last 160 million years. Measurements of  $^{4}\text{He}$ , and U isotopes from the fossil corals agree with a previously published suite of diagenetic tests on the same sample suite indicating that these scleractinian corals preserve primary geochemical records of ancient seawater and coral calcification (Gothmann et al., 2015, 2016, 2017). U/Ca ratios measured in this suite of coral samples show a factor of 4–5 increase between the early Cenozoic and today. We interpret this increase as reflecting both an increase in seawater [U] as well as a decline in seawater [Ca].

We find that the observed increase in seawater [U] between the early Cenozoic and present is consistent with a carbonate ion control over U removal rates, as originally suggested by Broecker (1971). Fossil coral U/Ca data are also compatible with the hypothesis that rates of low-temperature hydrothermal alteration have decreased by a factor of 2 between the early Cenozoic and today, as modeled by Higgins and Schrag (2015). Finally, our coral data are in agreement with previous reconstructions of Cenozoic seawater U isotopes from Goto et al. (2014) and Wang et al. (2016a), suggesting that changes in suboxic and anoxic seafloor area may play a role in driving seawater uranium variations over the Cenozoic. Overall, our results suggest that a diverse range of factors including uranium complexation chemistry, ocean oxygenation, and hydrothermal processes could be responsible for driving variations in Cenozoic seawater uranium concentration and isotopic compositions. While our data can place limits on the importance of these mechanisms, it is not currently possible to rule out any of the abovementioned controls. We also note that these controls may be important to consider when evaluating other reconstructions of uranium concentrations and isotopes.

#### ACKNOWLEDGEMENTS

We would like to thank Francois L.H. Tissot for helpful comments on multiple drafts of this manuscript as well as Associate Editor, Claudine Stirling, and an anonymous reviewer. We thank Stephen Cairns and Tim Cofer (Smithsonian Institution), Linda Ivany (Syracuse University), Roger Portell (Florida Museum of Natural History), Anne Cohen and Bill Thompson (WHOI), the USGS, and Gregory Dietl (Paleontological Research Institution) for loaning samples. Elizabeth Lundstrom (Princeton University) and Lindsey Hedges (California Institute of Technology) provided critical analytical support. We also thank Sarah Jane White (USGS), Francois Morel (Princeton University) and Will Amidon (Middlebury College) for helpful discussions that improved this manuscript.

## APPENDIX A. SUPPLEMENTARY MATERIAL

Supplementary data to this article can be found online at <https://doi.org/10.1016/j.gca.2019.01.039>.

## REFERENCES

Amidon W. H., Hobbs D. and Hynek S. A. (2015) Retention of cosmogenic  ${}^3\text{He}$  in calcite. *Quat. Geochronol.* **27**, 172–184.

Anagnostou E., Sherrell R. M., Gagnon A. C., LaVigne M., Field M. P. and McDonough W. F. (2011) Seawater nutrient and carbonate ion concentrations recorded as P/Ca, Ba/Ca, and U/Ca in the deep-sea coral *Desmophyllum dianthus*. *Geochim. Cosmochim. Acta* **75**, 2529–2543.

Andersen M. B., Elliot T., Freymuth H., Sims K. W. W., Niu Y. and Kelley K. A. (2015) The terrestrial uranium isotope cycle. *Nature* **517**, 356–359.

Andersen M. B., Stirling C. H., Zimmermann B. and Halliday A. (2010) Precise determination of the open ocean  ${}^{234}\text{U}/{}^{238}\text{U}$  composition. *Geochim. Geophys. Geosyst.* **11**, Q12003.

Andersen M. B., Vance D., Morford J. L., Bura-Nakic E., Breitenbach S. F. M. and Och L. (2016) Closing in on the marine  ${}^{238}\text{U}/{}^{235}\text{U}$  budget. *Chem. Geol.* **420**, 11–22.

Anderson R. F. (1987) Redox behavior of uranium in an anoxic marine basin. *Uranium* **3**, 145–164.

Anderson R. F., LeHuray A. P., Fleisher M. Q. and Murray J. W. (1989) Uranium deposition in Saanich Inlet sediments, Vancouver Island. *Geochim. Cosmochim. Acta* **53**, 2205–2213.

Anderson R. F., Bacon M. P. and Brewer P. G. (1982) Elevated Concentrations of Actinides in Mono Lake. *Science* **216**, 514–516.

Armid A., Takaesu Y., Fahmiati T., Yoshida S., Hanashiro R., Fujimura H., Higuchi T., Taira E. and Oomori T. (2008) U/Ca as a possible proxy of carbonate system in coral reef. In *Proceedings of the 11th International Coral Reef Symposium*, pp. 92–96.

Barnes C. E. and Cochran J. K. (1990) Uranium removal in oceanic sediments and the oceanic U balance. *Earth Planet. Sci. Lett.* **97**, 94–101.

Basu A., Sanford R. A., Johnson T. M., Lundstrom C. C. and Loffler F. E. (2014) Uranium isotopic fractionation factors during U(VI) reduction by bacterial isolates. *Geochim. Cosmochim. Acta* **136**, 100–113.

Belli K. M., DiChristina T. J., Van Cappellen P. and Taillefert M. (2015) Effects of aqueous uranyl speciation on the kinetics of microbial uranium reduction. *Geochim. Cosmochim. Acta* **157**, 109–124.

Bender M. L. (1973) Helium-uranium dating of corals. *Geochim. Cosmochim. Acta* **37**, 1229–1247.

Berner R. A. (1981) A new geochemical classification of sedimentary environments. *J. Sediment. Res.* **51**, 359–365.

Bernhard G., Geipel G., Reich T., Brendler V., Amayri S. and Nitsche H. (2001) Uranyl(VI) carbonate complex formation: Validation of the  $\text{Ca}_2\text{UO}_2(\text{CO}_3)_3(\text{aq})$  species. *Radiochim. Acta* **89**, 511–518.

Bigeleisen J. (1996) Nuclear size and shape effects in chemical reactions. Isotope chemistry of the heavy elements. *J. Am. Chem. Soc.* **118**, 3676–3680.

Brennan S. T., Lowenstein T. K. and Cendón D. I. (2013) The major-ion composition of Cenozoic seawater: The past 26 million years from fluid inclusions in marine halite. *Am. J. Sci.* **313**, 713–775.

Brennecke G. A., Herrmann A. D., Algeo T. J. and Anbar A. D. (2011) Rapid expansion of oceanic anoxia immediately before the end-Permian mass extinction. *Proc. National Acad. Sci.* **108**, 17631–17634.

Broecker W. S. (1971) A kinetic model for the chemical composition of sea water. *Quat. Res.* **1**, 188–207.

Broecker W. (2013) How to think about the evolution of the ratio of Mg to Ca in seawater. *Am. J. Sci.* **313**, 776–789.

Brown S. T., Basu A., Ding X., Christensen J. N. and DePaolo D. J. (2018) Uranium isotope fractionation by abiotic reductive precipitation. *Proc. Natl. Acad. Sci.* **35**, 8688–8693.

Chabaux F., Riote J., Clauer N. and France-Lanord C. (2001) Isotopic tracing of the dissolved U fluxes of Himalayan rivers: implications for present and past U budgets of the Ganges-Brahmaputra system. *Geochim. Cosmochim. Acta* **65**, 3201–3217.

Chen J. H., Edwards R. L. and Wasserburg G. J. (1986)  ${}^{238}\text{U}$ ,  ${}^{234}\text{U}$  and  ${}^{232}\text{Th}$  in seawater. *Earth Planet. Sci. Lett.* **80**, 241–251.

Chen X., Romaniello S. J., Herrmann A. D., Wasylewski L. E. and Anbar A. D. (2016) Uranium isotope fractionation during coprecipitation with aragonite and calcite. *Geochim. Cosmochim. Acta* **188**, 189–208.

Chen X., Romaniello S. J. and Anbar A. D. (2017) Uranium isotope fractionation induced by aqueous speciation: Implications for U isotopes in marine  $\text{CaCO}_3$  as a paleoredox proxy. *Geochim. Cosmochim. Acta* **215**, 162–172.

Chen X., Romaniello S. J., Herrmann A. D., Hadisty D., Gill B. C. and Anbar A. D. (2018a) Diagenetic effects on uranium isotope fractionation in carbonate sediments from the Bahamas. *Geochim. Cosmochim. Acta* **237**, 294–311.

Chen X., Romaniello S. J., Herrmann A. D., Samankassou E. and Anbar A. D. (2018b) Biological effects on uranium isotope fractionation ( ${}^{238}\text{U}/{}^{235}\text{U}$ ) in primary biogenic carbonates. *Geochimica et Cosmochimica Acta* **240**, 1–10.

Cheng H., Adkins J. F., Edwards R. L. and Boyle E. A. (2000) U-Th dating of deep-sea corals. *Geochim. Cosmochim. Acta* **64**, 2401–2416.

Cherniak D. J., Amidon W., Hobbs D. and Watson E. B. (2015) Diffusion of helium in carbonates: Effects of mineral structure and composition. *Geochim. Cosmochim. Acta* **165**, 449–465.

Chutcharavan P. M., Dutton A. and Ellwood M. J. (2018) Seawater  ${}^{234}\text{U}/{}^{238}\text{U}$  recorded by modern and fossil corals. *Geochim. Cosmochim. Acta* **224**, 1–17.

Clarkson M. O., Stirling C. H., Jenkyns H. C., Dickson A. J., Procelli D., Moy C. M., Pogge von Strandmann P. A. E., Cooke I. R. and Lenton T. M. (2018) Uranium isotope evidence for two episodes of deoxygenation during Oceanic Anoxic Event 2. *Proc. Natl. Acad. Sci.* **115**, 2918–2923.

Cochran J. K. (1982) The oceanic chemistry of the U- and Th-series nuclides. In *Uranium Series Disequilibrium: Applications to Environmental Problems* (eds. M. Ivanovich and R. S. Harmon). Clarendon, Oxford, pp. 384–430.

Cochran J. K., Carey A. E., Sholkovitz E. R. and Surprenant L. D. (1986) The geochemistry of uranium and thorium in coastal marine sediments and sediment pore waters. *Geochim. Cosmochim. Acta* **50**, 663–680.

Coggon R. M., Teagle D. A. H., Smith-Duque C. E., Alt J. C. and Cooper M. J. (2010) Reconstructing past seawater Mg/Ca and Sr/Ca from mid-ocean ridge flank calcium carbonate veins. *Science* **327**, 1114–1117.

Copeland P., Watson E. B., Urizar S. F., Patterson D. and Lapan T. J. (2007) Alpha thermochronology of carbonates. *Geochim. Cosmochim. Acta* **71**, 4488–4511.

Cros A., Gautheron C., Pagel M., Berthet P., Tassan-Got L., Douville E., Pinna-Jamme R. and Sarda P. (2014)  ${}^4\text{He}$  behavior in calcite filling viewed by (U-Th)/He dating,  ${}^4\text{He}$  diffusion and crystallographic studies. *Geochim. Cosmochim. Acta* **125**, 414–432.

Crusius J., Calvert S., Pedersen T. and Sage D. (1996) Rhenium and molybdenum enrichments in sediments as indicators of

oxic, suboxic and sulfidic conditions of deposition. *Earth Planet. Sci. Lett.* **145**, 65–78.

DeCarlo T. M., Gaetani G. A., Holcomb M. and Cohen A. L. (2015) Experimental determination of factors controlling U/Ca of aragonite precipitated from seawater: Implications for interpreting coral skeleton. *Geochim. Cosmochim. Acta* **162**, 151–165.

Dickson J. A. D. (2002) Fossil echinoderms as monitor of the Mg/Ca ratio of Phanerozoic Oceans. *Science* **298**, 1222–1224.

Dickson J. A. D. (2004) Echinoderm skeletal preservation: calcite–aragonite seas and the Mg/Ca ratio of Phanerozoic oceans. *J. Sediment. Res.* **74**, 355–365.

Djogic R., Sipos L. and Branica M. (1986) Characterization of uranium(VI) in seawater. *Limnol. Oceanography* **31**, 1122–1131.

Dong W. and Brooks S. C. (2006) Determination of the formation constants of ternary complexes of uranyl and carbonate with alkaline earth metals ( $Mg^{2+}$ ,  $Ca^{2+}$ ,  $Sr^{2+}$ , and  $Ba^{2+}$ ) using anion exchange method. *Environ. Sci. Technol.* **40**, 4689–4695.

Dunk R. M., Mills R. A. and Jenkins W. J. (2002) A reevaluation of the oceanic uranium budget for the Holocene. *Chem. Geol.* **190**, 45–67.

Elderfield H. and Schultz A. (1996) Mid-ocean ridge hydrothermal fluxes and the chemical composition of the ocean. *Ann. Rev. Earth Planetary Sci.* **24**, 191–224.

Endrizzi F., Leggett C. J. and Rao L. (2016) Scientific basis for efficient extraction of uranium from seawater. I: understanding the chemical speciation of uranium under seawater conditions. *Ind. Eng. Chem. Res.* **55**, 4249–4256.

Endrizzi F. and Rao L. (2014) Chemical speciation of Uranium(VI) in marine environments: complexation of calcium and magnesium ions with  $[(UO_2)(CO_3)_3]^{4-}$  and the effect on the extraction of uranium from seawater. *Chem. - A Eur. J.* **20**, 14499–14506.

Esat T. M. and Yokoyama Y. (2006) Variability in the uranium isotopic composition of the oceans over glacial-interglacial timescales. *Geochim. Cosmochim. Acta*, 4140–4150.

Fanale F. P. and Schaeffer O. A. (1965) Helium-uranium ratios for pleistocene and tertiary fossil aragonites. *Science* **149**, 312–316.

Farley K. A., Wolf R. A. and Silver L. T. (1996) The effects of long alpha-stopping distances on (U-Th)/He ages. *Geochim. Cosmochim. Acta* **60**, 4223–4229.

Gabitov R. I., Gaetani G. A., Watson E. B., Cohen A. L. and Ehrlich H. L. (2008) Experimental determination of growth rate effect on  $U^{6+}$  and  $Mg^{2+}$  partitioning between aragonite and fluid at elevated  $U^{6+}$  concentration. *Geochim. Cosmochim. Acta* **72**, 4058–4068.

Gothmann A. M., Stolarski J., Adkins J. F., Dennis K. J., Schrag D. P., Schoene B. and Bender M. L. (2015) Fossil corals as an archive of secular variations in seawater chemistry. *Geochim. Cosmochim. Acta* **160**, 188–208.

Gothmann A. M., Higgins J. A., Swart P. K., Giri S. J., Adkins J. F., Stolarski J., Blättler C. L. and Bender M. L. (2016) Calcium isotopes in fossil corals: implications for coral vital effects and biomineralization through time. *Earth Planet. Sci. Lett.* **444**, 205–214.

Gothmann A. M., Higgins J. A., Adkins J. F. and Stolarski J. (2017) A Cenozoic record of Mg isotopes from fossil corals. *Geology* **45**, 1039–1042.

Goto K. T., Anbar A. D., Gordon G. W., Romaniello S. J., Shimoda G., Takaya Y., Tokumaru A., Nozaki T., Suzuki K., Machida S., Hanyu T. and Usui A. (2014) Uranium isotope systematics of ferromanganese crusts in the Pacific Ocean: Implications for the marine  $^{238}U/^{235}U$  isotope system. *Geochim. Cosmochim. Acta* **146**, 43–58.

Hain M. P., Sigman D. M., Higgins J. A. and Haug G. H. (2015) The effects of secular calcium and magnesium concentration changes on the thermodynamics of seawater acid/base chemistry: Implications for Eocene and Cretaceous ocean carbon chemistry and buffering. *Global Biogeochem. Cycles* **29**, 517–533.

Hart S. R. and Staudigel H. (1982) The control of alkalies and uranium in seawater by ocean crust alteration. *Earth Planet. Sci. Lett.* **58**, 202–212.

Henderson G. M. and Anderson R. F. (2003) The U-series toolbox for paleoceanography. *Rev. Mineral. Geochem.* **52**, 493–531.

Higgins J. A. and Schrag D. P. (2015) The Mg isotopic composition of Cenozoic seawater – evidence for a link between Mg-clays, seawater Mg/Ca, and climate. *Earth Planet. Sci. Lett.* **416**, 73–81.

Hönisch B., Ridgwell A., Schmidt D. N., Thomas E., Gibbs S. J., Sluijs A., Zeebe R. E., Kump L., Martindale R. C., Greene S. E., Kiessling W., Ries J., Zachos J. C., Royer D. L., Barker S., Marchitto, Jr., T. M., Moyer R., Pelejero C., Ziveri P., Foster G. L. and Williams B. (2012) The geological record of ocean acidification. *Science* **335**, 1058–1063.

Horita J., Zimmermann H. and Holland H. D. (2002) Chemical evolution of seawater during the Phanerozoic: implications from the record of marine evaporites. *Geochim. Cosmochim. Acta* **66**, 3733–3756.

Hua B., Xu H., Terry J. and Deng B. (2006) Kinetics of Uranium (VI) Reduction by Hydrogen Sulfide in Anoxic Aqueous Systems. *Environ. Sci. Technol.* **40**, 4666–4671.

James R. H., Allen D. E. and Seyfried W. E. (2003) An experimental study of alteration of oceanic crust and terrigenous sediments at moderate temperatures (51 to 350°C) insights as to chemical processes in near-shore ridge-flank hydrothermal systems. *Geochim. Cosmochim. Acta* **67**, 681–691.

Inoue M., Suwa R., Suzuki A., Sakai K. and Kawahata H. (2011) Effects of seawater pH on growth and skeletal U/Ca ratios of *Acropora digitifera* coral polyps. *Geophys. Res. Lett.* **38**, 12801–12804.

Kendall B., Brennecke G. A., Weyer S. and Anbar A. D. (2013) Uranium isotope fractionation suggests oxidative uranium mobilization at 2.50 Ga. *Chem. Geol.* **362**, 105–114.

Keul N., Langer G., de Nooijer L., Nehrke G., Reichtart F.-J. and Bijma J. (2013) Incorporation of uranium in benthic foraminiferal calcite reflects seawater carbonate ion concentration. *Geochim. Geophys. Geosyst.* **G3**(14), 102–111.

Klinkhammer G. P. and Palmer M. R. (1991) Uranium in the oceans: Where it goes and why. *Geochim. Cosmochim. Acta* **55**, 1799–1806.

Ku T. (1965) An evaluation of the  $U^{234}/U^{238}$  method as a tool for dating pelagic sediments. *J. Geophys. Res.*, 3457–3474.

Langmuir D. (1978) Uranium solution-mineral equilibria at low temperatures with applications to sedimentary ore deposits. *Geochim. Cosmochim. Acta* **42**, 547.

Linhoff B. S., Bennett P. C., Puntsag T. and Gerel O. (2011) Geochemical evolution of uraniferous soda lakes in Eastern Mongolia. *Environ. Earth Sci.* **62**, 171–183.

Lovley D. R., Phillips E. J. P., Gorby Y. A. and Landa E. R. (1991) Microbial reduction of uranium. *Nature* **350**, 413–416.

Lovley D. R. and Phillips E. J. P. (1992) Reduction of uranium by Desulfovibrio desulfuricans. *Appl. Environ. Microbiol.* **58**, 850–856.

Lowenstein T. K., Hardie L. A., Brennan S. T., Hardie L. A. and Demicco R. V. (2001) Oscillations in Phanerozoic seawater chemistry. Evidence from fluid inclusions. *Science* **294**, 1086–1088.

Lowenstein T. K., Hardie L. A., Timofejeff M. N. and Demicco R. V. (2003) Secular variation in seawater chemistry and the origin of calcium chloride basinal brines. *Geology* **31**, 857–860.

MacDougall (1977) Uranium in marine basalts. Concentration, distribution and implications. *Earth Planet. Sci. Lett.* **35**, 65–70.

McManus J., Berelson W. M., Klinkhammer G. P., Hammond D. E. and Holm C. (2005) Authigenic uranium. Relationship to oxygen penetration depth and organic carbon rain. *Geochim. Cosmochim. Acta* **69**, 95–108.

McManus J., Berelson W. M., Severmann S., Poulsen R. L., Hammond D. E., Klinkhammer G. P. and Holm C. (2006) Molybdenum and uranium geochemistry in continental margin sediments. Paleoproxy potential. *Geochim. Cosmochim. Acta* **70**, 4643–4662.

Meece D. E. and Benninger L. K. (1993) The coprecipitation of Pu and other radionuclides with  $\text{CaCO}_3$ . *Geochim. Cosmochim. Acta* **57**, 1447–1458.

Michard A. and Albarede F. (1985) Hydrothermal uranium uptake at ridge crests. *Nature* **317**, 244–246.

Michard A., Albarede F., Michard G., Minster J. F. and Charlou J. L. (1983) Rare-earth elements and uranium in high-temperature solutions from East Pacific Rise hydrothermal vent field (13°N). *Nature* **303**, 795–797.

Milliman J. D. (1993) Production and accumulation of calcium carbonate in the ocean: Budget of a nonsteady state. *Global Biogeochem. Cycles* **7**, 927–957.

Mills R. A. and Dunk R. M. (2010) Tracing low-temperature fluid flow on ridge flanks with sedimentary uranium distribution. *Geochem. Geophys. Geosyst.* **11**, Q08009.

Min G. R., Edwards R. L., Taylor F. W., Recy J., Gallup C. D. and Beck J. W. (1995) Annual cycles of U/Ca in coral skeletons and U/Ca thermometry. *Geochim. Cosmochim. Acta* **59**, 2025–2042.

Montoya-Pino C., Weyer S., Anbar A. D., Pross J., Oschmann W., van de Schootbrugge B. and Arz H. W. (2010) Global enhancement of ocean anoxia during Oceanic Anoxic Event 2: A quantitative approach using U isotopes. *Geology* **38**, 315–318.

Morford J. L. and Emerson S. (1999) The geochemistry of redox sensitive trace metals in sediments. *Geochim. Cosmochim. Acta* **63**, 1735–1750.

Morford J. L., Martin W. R. and Carney C. M. (2009) Uranium diagenesis in sediments underlying bottom waters with high oxygen content. *Geochim. Cosmochim. Acta* **73**, 2920–2937.

Noordmann J., Weyer S., Georg R. B., Jöns S. and Sharma M. (2015)  $^{238}\text{U}/^{235}\text{U}$  isotope ratios of crustal material, rivers and products of hydrothermal alteration: new insights on the oceanic U isotope mass balance. *Isot. Environ. Health Stud.* **1**–23.

Palmer M. R. and Edmond J. M. (1989) The strontium isotope budget of the modern ocean. *Earth Planet. Sci. Lett.* **92**, 11–26.

Palmer M. R. and Edmond J. M. (1993) Uranium in river water. *Geochim. Cosmochim. Acta* **57**, 4947–4955.

Pogge von Strandmann P. A. E., Burton K. W., James R. H., van Calsteren P. and Gislason S. R. (2010) Assessing the role of climate on uranium and lithium isotope behaviour in rivers draining a basaltic terrain. *Chem. Geol.* **270**, 227–239.

Raddatz J., Rüggeberg A., Flögel S., Hathorne E. C., Liebetrau V., Eisenheuer A. and Dullo W.-C. (2014) The influence of seawater pH on U/Ca ratios in the scleractinian cold-water coral *Lophelia pertusa*. *Biogeosciences* **11**, 1863–1871.

Rausch S., Böhm F., Bach W., Klugel A. and Eisenhauer A. (2013) Calcium carbonate veins in ocean crust record a threefold increase of seawater Mg/Ca in the past 30 million years. *Earth Planet. Sci. Lett.* **362**, 215–224.

Reeder R. J., Nugent M., Lamble G. M., Tait C. D. and Morris D. E. (2000) Uranyl Incorporation in Calcite and Aragonite: XAFS and Luminescence Studies. *Environ. Sci. Technol.* **34**, 638–644.

Ridgwell A. (2005) A Mid Mesozoic Revolution in the regulation of ocean chemistry. *Mar. Geol.* **217**, 339–357.

Robinson L. F., Adkins J. F., Fernandez D. P., Burnett D. S., Wang S.-L., Gagnon A. C. and Krakauer N. (2006) Primary U distribution in scleractinian corals and its implications for U series dating. *Geochim. Geophys. Geosyst.* **7**, Q05022.

Romanillo S. J., Herrmann A. D. and Anbar A. D. (2013) Uranium concentrations and  $^{238}\text{U}/^{235}\text{U}$  isotope ratios in modern carbonates from the Bahamas: Assessing a novel paleoredox proxy. *Chem. Geol.* **362**, 305–316.

Roniewicz E. and Stolarski J. (1999) Evolutionary trends in the epithecate scleractinian corals. *Acta Palaeontol. Pol.* **44**, 131–166.

Rosenthal Y., Field M. P. and Sherrell R. M. (1999) Precise determination of element/calcium ratios in calcareous samples using sector field inductively coupled plasma mass spectrometry. *Anal. Chem.* **71**, 3248–3253.

Russell A. D., Emerson S., Nelson B. K., Erez J. and Lea D. W. (1994) Uranium in foraminiferal calcite as a recorder of seawater uranium concentrations. *Geochim. Cosmochim. Acta* **58**, 671–681.

Sarmiento J. and Gruber N. (2006) *Ocean Biogeochemical Dynamics*. Princeton University Press, Princeton, NJ.

Sarin M. M., Krishnaswami S., Somayajulu B. L. K. and Moore W. S. (1990) Chemistry of uranium, thorium, and radium isotopes in the Ganga-Brahmaputra river system: Weathering processes and fluxes to the Bay of Bengal. *Geochim. Cosmochim. Acta* **54**, 1387–1396.

Schauble E. A. (2007) Role of nuclear volume in driving equilibrium stable isotope fractionation of mercury, thallium, and other very heavy elements. *Geochim. Cosmochim. Acta* **71**, 2170–2189.

Schroeder J. H., Miller D. S. and Friedman G. M. (1970) Uranium distributions in recent skeletal carbonates. *J. Sediment. Petrol.* **40**, 672–681.

Shen G. T. and Dunbar R. B. (1995) Environmental controls on uranium in reef corals. *Geochim. Cosmochim. Acta* **59**, 2009–2024.

Shvartsev S. L., Isupov V. P., Vladimirov A. G., Kolpakova M. N., Ariunbileg S., Shatskaya S. S. and Moroz E. N. (2012) Lithium and uranium in closed Lake of Western Mongolia. *Chem. Sustain. Dev.* **20**, 37–42.

Simpson H. J., Trier R. M., Toggweiler J. R., Mathieu G., Deck B. L., Olsen C. R., Hammond D. E., Fuller C. and Ku T. L. (1982) Radionuclides in Mono Lake, California. *Science* **216**, 512–514.

Stirling C. H., Andersen M. B., Potter E. and Halliday A. N. (2007) Low-temperature isotopic fractionation of uranium. *Earth Planet. Sci. Lett.* **264**, 208–225.

Stirling C. H., Andersen M. B., Warthmann R. and Halliday A. N. (2015) Isotope fractionation of  $^{238}\text{U}$  and  $^{235}\text{U}$  during biologically-mediated uranium reduction. *Geochim. Cosmochim. Acta* **163**, 200–218.

Stylo M., Neubert N., Wang Y., Monga N., Romanillo S. J., Weyer S. and Bernier-Latmani R. (2015) Uranium isotopes fingerprint biotic reduction. *Proc. Natl. Acad. Sci.* **112**, 5619–5624.

Swart P. K. and Hubbard J. A. E. B. (1982) Uranium in scleractinian coral skeletons. *Coral Reefs* **1**, 13–19.

Thompson W. G., Spiegelman W., Goldstein S. L. and Speed R. C. (2003) An open-system model for U-series age determinations of fossil corals. *Earth Planet. Sci. Lett.* **210**, 365–381.

Thurber D. (1965) The concentrations of some natural radioelements in the water of the great basin. *Bull. Volcanol.* **28**, 195–201.

Timofeeff M. N., Lowenstein T. K., Martins da Silva M. A. and Harris N. B. (2006) Secular variation in the major-ion chemistry of seawater. Evidence from fluid inclusions in Cretaceous halites. *Geochim. Cosmochim. Acta* **70**, 1977–1994.

Tissot F. L. H. and Dauphas N. (2015) Uranium isotopic compositions of the crust and ocean: Age corrections, U budget and global extent of modern anoxia. *Geochim. Cosmochim. Acta* **167**, 113–143.

Tissot F. L. H., Chen C., Go B. M., Naziemiec M., Healy G., Bekker A., Swart P. K. and Dauphas N. (2018) Controls of eustasy and diagenesis on the  $^{238}\text{U}/^{235}\text{U}$  of carbonates and evolution of the seawater ( $^{234}\text{U}/^{238}\text{U}$ ) during the last 1.4 Myr. *Geochim. Cosmochim. Acta* **242**, 233–265.

Tyrrell T. and Zeebe R. E. (2004) History of carbonate ion concentration over the last 100 million years. *Geochim. Cosmochim. Acta* **68**, 3521–3530.

Wang X., Planavsky N. J., Reinhard C. T., Hein J. R. and Johnson T. M. (2016a) A Cenozoic seawater redox record derived from  $^{238}\text{U}/^{235}\text{U}$  in ferromanganese crusts. *Am. J. Sci.* **316**, 64–83.

Wang X., Reinhard C. T., Planavsky N. J., Owens J. D., Lyons T. W. and Johnson T. M. (2016b) Sedimentary chromium isotopic compositions across the Cretaceous OAE2 at Demerara Rise Site 1258. *Chem. Geol.* **429**, 85–92.

Wazne M., Korfiatis G. P. and Meng X. (2003) Carbonate effects on hexavalent uranium adsorption by iron oxyhydroxide. *Environ. Sci. Technol.* **37**, 3619–3624.

Weyer S., Anbar A. D., Gerdes A., Gordon G. W., Algeo T. J. and Boyle E. A. (2008) Natural fractionation of  $^{238}\text{U}/^{235}\text{U}$ . *Geochim. Cosmochim. Acta* **72**, 345–359.

Wheat C. G., Jannasch H. W., Kastner M., Plant J. N. and DeCarlo E. H. (2003) Seawater transport and reaction in upper oceanic basaltic basement: chemical data from continuous monitoring of sealed boreholes in a ridge flank environment. *Earth Planet. Sci. Lett.* **216**, 549–564.

Zeebe R. E. (2012) History of seawater carbonate chemistry, atmospheric  $\text{CO}_2$ , and ocean acidification. *Annu. Rev. Earth Planet. Sci.* **40**, 141–165.

Zheng Y., Anderson R. F., van Geen A. and Fleisher M. Q. (2002) Preservation of particulate non-lithogenic uranium in marine sediments. *Geochim. Cosmochim. Acta* **66**, 3085–3092.

Zimmermann H. (2000) Tertiary seawater chemistry - Implications from fluid inclusions in primary marine halite. *Am. J. Sci.* **300**, 723–767.

Associate editor: Claudine Stirling